Science Advances
AAAS

# Supplementary Materials for

## Distributed direct air capture by carbon nanofiber air filters

Ronghui Wu *et al.*

Corresponding author: Po-Chun Hsu, pochunhsu@uchicago.edu

*Sci. Adv.* **11**, eadv6846 (2025)
DOI: 10.1126/sciadv.adv6846

**This PDF file includes:**

**Supplementary Text 1**

Calculation of potential $CO_2$ mitigation amount

The potential annual $CO_2$ mitigation amount by air filter system (m) is calculated based on the assumption that per person receives 15 cfm in an indoor environment (*57*). Each person spent 90% of their time indoors (*9, 10*). The ventilation system runs 12 hours per day.

$$m = 0.9nv\rho C_{CO2} \times 12 \times 365 \quad \textbf{(S1)}$$

where n is the population, *v* is the flow rate, which is 25.5 $m^3/h$ (15 cfm), ρ is the $CO_2$ density at atmospheric pressure (1 bar) and temperature (25°C), $C_{CO2}$ is the concentration of $CO_2$, which is set as 420 ppm (*2*). The total global removal potential is calculated based on the world population in 2020. The population distribution used for calculating Fig. 1B is from the US Census Bureau of 2010. The map template is from https://commons.wikimedia.org/wiki/File:USA_Counties_with_FIPS_and_names.svg.

**Supplementary Text 2**

Calculation of theoretical temperature of CNF

Consider CNF whose temperature is $T_{CNF}$, and spectral emissivity is $\epsilon_{CNF}(\lambda) = 0.9$. It is subject to solar irradiance, atmospheric thermal radiation (corresponding to ambient air temperature $T_{amb}$), radiation emittance to the environment, and conductive and convective heat transfer. Assuming the adsorbent is at a thermal equilibrium state, the theoretical CNF temperature can be calculated by solving the following equation:

$$P_{CNF\_Quartz} - P_{sun} + P_{cond+conv} = 0 \quad \textbf{(S2)}$$

$P_{CNF\_Quartz}$ is the net radiation change between CNF and quartz surfaces:

$$P_{CNF\_Quartz} = \frac{\sigma(T_1^4 - T_2^4)}{\frac{1-\varepsilon_1}{\varepsilon_1 A_1} - \frac{1}{A_1 F_{12}} - \frac{1-\varepsilon_2}{\varepsilon_2 A_2}} \quad \textbf{(S3)}$$

where $\sigma$ is Stefan-Boltzmann constant; $T_1$ and $T_2$ are the temperatures of CNF and quartz tube, respectively; $\varepsilon_1$ and $\varepsilon_2$ are the emissivity of CNF and quartz tube; $A_1$ and $A_2$ are the areas of CNF and quartz tube; $F_{12}$ is the view factor from CNF to quartz tube, which is unity in our calculation.

$P_{sun}$ is the incident solar power:

$$P_{sun} = A_{CNF} \cdot SA \cdot I_{solar} \quad \textbf{(S4)}$$

$I_{solar}$ is solar irradiance. $A_{CNF}$ is the area of CNF. $SA$ is the solar absorptivity of CNF, which is 94.4% when the pyrolyze temperature is 900˚C, based on the experimental results.

$P_{cond+conv}$ is the power lost owing to convection and conduction:

$$P_{cond+conv}(T_{adsorbent}, T_{amb}) = h_c(T_{CNF} - T_{amb}) \quad \textbf{(S5)}$$

Where $h_c$ is a combined non-radiative heat coefficient that captures the collective effect of conduction and convection. Here, the $h_c$ is assumed to be 8 W/ ($m^2$·K).

**Supplementary Text 3**

Life cycle assessment of DAC air filter

**Goal and scope.** The overall goals of the life cycle assessment of the DAC air filter can be divided into the following three points: First, evaluation of the greenhouse gas emission impacts of CNF-based adsorbents and comparison with three other adsorbents using the same PEI mass loading. Second, assessment of the carbon footprint of captured $CO_2$ from cradle-to-gate and cradle-to-grave, therefore, analyze the carbon footprint of each step for $CO_2$ capture and storage, including adsorbent, transport, regeneration, pressure drop, vacuum supply, and storage. In addition, calculate the overall direct air capture efficiency and cradle-to-grave efficiency. Third, compare the environmental impacts of CNF-based adsorbents using two different regeneration methods (solar thermal, electrothermal) and four different renewable resources (hydro, wind, photovoltaic, and geothermal).

**Scenario description.** PEI is chosen to be loaded on four different substrates, i.e., CNF, alumina, silica, and cellulose. CNF is fabricated by oxidation and pyrolysis of PAN nanofiber, with a carbon yield of 56% (experimental data). The mass ratio for PEI and substrate is 61: 39, consistent with the experimental data for DAC air filter design. 1 kg of carbon nanofiber air filter was assumed to capture 133 kg of $CO_2$ in its lifetime. To fabricate 1 kg of air filter, 0.61kg PEI and 0.39kg CNF are needed. CNF/PEI adsorbent is chosen for the DAC air filter in the building ventilation system. The energy for pressure drop ($E_{pressure\ drop}$) is calculated by:

$$E_{pressure\ drop} = \frac{PvSt}{1000 \times N} \quad \textbf{(S6)}$$

where P is the pressure drop for the air filter, and S is the area of the air filter, which is 0.65 $m^2$. $v$ is the face velocity, and t is the usage time for the air filter. N is the total $CO_2$ mass. The calculated energy for pressure drop is 0.98 kWh/kg $CO_2$. The regeneration energy using electrothermal technology is calculated based on the experimental data in Fig. 3F. The energy for the required vacuum in collecting the regenerated $CO_2$ is 0.063 kWh/kg $CO_2$ (*64*). The air filter is transported to the city's centralized spot for generation, which is set as 10 km away from buildings on average. After regeneration, $CO_2$ gas was compressed to a desired pressure and transported to the storage well for sequestration. The $CO_2$ is transported to the drilling well using a pipeline (Tables S9-10). The $CO_2$ will be recompressed every 200 km during transportation (*55*). It is assumed that 60% of the regeneration spots are 180 km away from the nearest sequestration location, and the other 40% are 500 km on average (*65*). $CO_2$ is compressed and injected into geological formations, including depleted oil and gas reservoirs, deep coal seams, and saline aquifers. The energy to achieve an injection pressure from 1 to 150 bar is 0.101 kWh/$CO_2$ (*54*). We assume that 128 drilling wells with 2000m depths are constructed for $CO_2$ storage. The lifetime for the drilling wells is 30 years.

**System boundaries.** Based on the goals of our LCA study, we distinguish between cradle-to-gate (adsorbent ready to use for removing 1 kg $CO_2$) and cradle-to-grave system (capturing and storing 1 kg $CO_2$ geologically) boundaries (Fig.4A): Cradle-to-gate boundary includes adsorbent production and end-of-life disposal. Cradle-to-grave boundary covers the cradle-to-gate, DAC operation, and $CO_2$ storage process. The energy consumption for DAC operation includes air filter pressure drop, transportation of air filter, regeneration, and vacuum pumping, and the $CO_2$ storage process includes gas transportation, $CO_2$ compression, and deep underground injection.

**Life-cycle inventory (LCI).** The LCI data are described in Table S1-S11. The flow for inputs and outputs was taken from the *Ecoinvent 3.1* database. All mass and energy flows are analyzed

for flows entering and leaving the system boundaries. LCI data on the US level, and if the corresponding data are not available, on a global (GLO) or rest of world (RoW) level.

**Environmental impact assessment.** In this study, the environmental impacts were categorized into 4 midpoint indicators using The International Reference Life Cycle Data System (ILCD) 2011, including GHG emissions (Fig.4C), land use (Fig.4E), freshwater ecotoxicity (Fig.4F), and human body ecotoxicity (Fig.S10), in eliminating 1 kg of $CO_2$.

**Sensitivity analysis.** Sensitivity analyses were evaluated to examine how variations in key parameters could affect the baseline life cycle estimates.

1. Solvent in electrospinning. The fabrication of carbon nanofibers involves electrospinning of PAN, which was dissolved in dimethylformamide (DMF) in our experiment. DMF can be replaced by a greener solvent, dimethyl sulfoxide (DMSO) in PAN electrospinning, as demonstrated by Lilia Sabantina et al. (*61*) As shown in Table S13, the environmental impacts of the adsorbent prepared using these two solvents are compared. When changing the solvent to DMSO, the $CO_2$ released in absorbing 1 kg of $CO_2$ cradle-to-gate decreases from 0.0492 kg to 0.0443 kg. Additionally, the $CO_2$ removal efficiency increases from 92.1% to 92.6%. In addition, other environmental factors, such as human toxicity, ionizing radiation, and marine eutrophication, have dramatically decreased. In particular, the impacts of ionization radiation on the ecosystem and marine eutrophication decreased by 21.5% and 25.6%, respectively.

2. Cyclability of the adsorbent. Amine adsorbent can be used repeatedly after regeneration. In the current assessment, 1 kg of adsorbent is assumed to have the capacity to absorb 133 kg of CO2 in its lifetime (*54*). In other words, with a capacity of 3 mmol/g, it can be recycled around 1000 times. To understand the sensitivity of the cyclability of cycling numbers in environmental impacts and carbon removal efficiency, we compared the scenarios where adsorbent recycled 500, 2000, and 4000 times, as shown in Table S14. In these three scenarios, the $CO_2$ released in absorbing 1 kg of $CO_2$ cradle-to-gate are 0.0983 kg, 0.0246 kg, and 0.0123 kg, respectively. The corresponding cradle-to-grave CO2 removal efficiencies are 87.2%, 94.5%, and 95.8%, respectively. Therefore, the sensitivity analysis reveals the importance of improving the cyclability of the adsorbent in increasing the overall carbon removal efficiency, which can be achieved by enhancing amine thermal stability and amine-support bonding (*24*).

3. Adsorption capacity. In CNF/PEI adsorbent, the PEI mass loading has a direct influence on the adsorbent's adsorption capacity, as shown in Figs. 2F-G and the discussion in the manuscript. Three scenarios with PEI loading of 48%, 61%, and 78%, which are correlated to capacities of 2.2 mmol/g, 3 mmol/g, and 4 mmol/g are assessed. As shown in Table S15, in these three scenarios, the $CO_2$ released in absorbing 1 kg of $CO_2$ cradle-to-gate are 0.0625 kg, 0.0492 kg, and 0.0407 kg. The cradle-to-grave $CO_2$ removal efficiencies are 90.8%, 92.1 %, and 93.0% respectively. Higher mass loading and adsorption capacity contribute to enhanced $CO_2$ removal efficiency.

**Other sensitivity and uncertainty**. Firstly, the energy consumption, raw materials for various adsorbents involved in this study were from different sources, which could introduce uncertainty. Secondly, assumptions were made in this study about transportation, regeneration, and the $CO_2$ storage process (see Scenario description section). Thirdly, though we demonstrated the high efficiency air filter regeneration using direct sunlight and joule heating, the air filter realized in this work was on gram scale; hence, there might be uncertainty when scaling up to ton scale.

**Supplementary Text 4**

Techno-economic analysis of DAC air filter

For a city with a population of 10 million, the mass flow of $CO_2$ is 2,053 tonne/day or 0.75 megatonne/year (Mt/year) (Please see detailed calculation in Supplementary Text 1). For simplicity, and to account for inefficiencies in distributed DAC $CO_2$ capture implantation, we assume a capture amount of 1,000 tonne/day. If filters are used on average for 50 cycles per year and capture 0.207 kg of $CO_2$ per cycle, around 35 million filters are required to capture this amount of $CO_2$.

In the TEA, the filter is assumed to have an area of 0.65 $m^2$ for a total filter mass of 1.57 kg; this was taken as a representative average of multiple filter dimensions similar to existing HVAC filters. A thin layer of polyester or similar material can be attached to the filter, allowing it to be used in existing HVAC systems without retrofitting or the use of an additional filter. Each filter captures 0.207 kg of $CO_2$ per day, after which it is saturated and must be replaced to continue capturing $CO_2$. We assume used filters accumulate before being returned in packs of seven (i.e., roughly every week) at nearby locations, such as a convenience store, where they can be exchanged for clean filters. We assume that filters are transported an average of 10 km to a filter regeneration facility, where the $CO_2$ is captured. Because the filters are assumed to be replaced roughly every week, they are assumed to be used about 50 times per year for a total number of 1000 cycles over a span of 20 years.

As mentioned in the main manuscript, the TEA consists of cash flow projections for 20 years, which are discounted into present value. The details of this analysis are described below, and a summary of the main TEA assumptions is shown in Table S16. The modeled cash expenses include direct costs, operating expenses (OPEX), and capital expenses (CAPEX), and the modeled cash revenue includes $CO_2$ sales and non-taxable income from 45Q credits for $CO_2$ capture and utilization.

Direct costs include raw materials, labor, heating expenses, and electricity that go into the manufacturing of the DAC filters or the capturing, utilization, and storage of $CO_2$. Electricity and heating expenses were assumed to be \$82.6/MWh and \$4/MMBtu, respectively, based on recently reported costs (*66, 67*). All of the chemicals required as raw materials are commodities widely available and, consequently, there should be no notable challenges associated with procuring raw materials or threats from supply chain disruptions; for this analysis, we used costs identified from the North American market shown in Table S17. CNF is assumed to have a recycling rate of 95% because of its robust thermal stability. For the labor, the filter production and $CO_2$ capture are expected to require 50 and 20 shifts per week (i.e., 50 and 20 full-time workers), where work per operator is 2,080 hours per year, and cost per worker including overhead is \$80/h.

OPEX includes sales, general, and administrative (SG&A) expenses, as well as transportation of both filters and $CO_2$, $CO_2$ compression, and $CO_2$ storage costs. Filters were assumed to be transported 1000 mi on average from the filter production facility to the city where they capture $CO_2$, and then an average of 10 km from the recollection facilities to the $CO_2$ capture plant; $CO_2$ is assumed to be transported 200 mi by pipeline to the site of $CO_2$ storage or utilization. With these assumptions, the resulting transportation costs are \$0.48/filter from the transportation of the production facility to the DAC city, \$31/tonne $CO_2$ for the back-and-forth transportation from the $CO_2$ point of capture and the regeneration facility, and \$17/tonne for $CO_2$ transportation to the point of storage or utilization (*68*). $CO_2$ compression is assumed to cost \$24 as is the case from high-purity sources like an ammonia plant (*69*), and $CO_2$ storage is assumed to cost \$10/tonne at

a site that sequesters at least 3 Mt/year of $CO_2$ from multiple sources (*68*). SG&A was assumed to be 20% of labor expenses.

Finally, CAPEX includes the purchase of equipment with lifetimes greater than one year, as well as land. The equipment includes furnaces and electrospinning equipment required to produce the filters and the vacuum pump for $CO_2$ extraction within the filter regeneration. The equipment costs are shown in Table S18.

The investments and costs used to fund the filter production and $CO_2$ capture are assumed to be 100% equity contributions. The cash flows are discounted with a nominal cost of equity rate of 10% ($r_n$) (*70*), and a real cost of 7.4% ($r_r$) assuming a 2.4% inflation based on recent derived values from 10-year Treasury Inflation-Protected Securities (TIPS) (*71*). In this work, 2024 was used as a basis year; thus, all revenue and costs throughout the project lifetime reflect the 2024 USD purchasing power.

The levelized cost of filter (LCOF) was estimated as

$$\mathrm{LCOF} = \frac{\sum_{t=0}^{t=20} \frac{(\mathrm{Direct\ Costs_t} + \mathrm{OPEX_t} + \mathrm{CAPEX_t})}{(1+r_n)^t}}{\sum_{t=0}^{t=20} \frac{\mathrm{filters_t}}{(1+r_r)^t}}. \quad \textbf{(S7)}$$

Here, the direct costs, OPEX, and CAPEX are discounted at the nominal cost of equity and the filters produced are discounted at the real cost of equity since we expect costs to remain constant on real terms (i.e., adjust only for inflation) throughout the 20 years modelled. The resulting cost per filter is approximately $21.

Similarly, the levelized cost of $CO_2$ capture ($LCCO_2$) was estimated as

$$\mathrm{LCCO2} = \frac{\sum_{t=0}^{t=20} \frac{(\mathrm{Direct\ Costs_t} + \mathrm{OPEX_t} + \mathrm{CAPEX_t})}{(1+r_n)^t}}{\sum_{t=0}^{t=20} \frac{\mathrm{CO_2\ captured_t}}{(1+r_r)^t}} \quad \textbf{(S8)}$$

where the costs extend from filter production all the way to $CO_2$ being recovered from the filters and compressed to 152 bars for transportation (*69*). This cost was estimated to compare with other $CO_2$ capture technologies.

To estimate the net cost of $CO_2$ capture, we additionally estimated the cost of $CO_2$ transportation, and either costs related to storage, or revenue from $CO_2$ sales (e.g., for enhanced oil recovery, EOR). The 45Q $CO_2$ capture credits were also subtracted from the cost. Overall, the net cost of capture was estimated as

$$\mathrm{Net\ cost} = \frac{\sum_{t=0}^{t=20} \frac{(\mathrm{Direct\ Costs_t} + \mathrm{OPEX_t} + \mathrm{CAPEX_t} - \mathrm{CO_2\ sales_t} - \mathrm{45Q\ credits_t})}{(1+r_n)^t}}{\sum_{t=0}^{t=20} \frac{\mathrm{CO_2\ captured_t}}{(1+r_r)^t}}. \quad \textbf{(S9)}$$

**Supplementary Text 5**

Sensitivity analysis on the net cost of $CO_2$ capture

To estimate the effect of key variables on the net cost of $CO_2$ capture (i.e., after DAC credits), particularly how much the cost of capture can change between lower and upper bounds of these variables, a sensitivity analysis was conducted for electricity cost, model discount rate, filter production cost, as well as number of times the filter is regenerated per year. We analyzed filter regeneration and not replacement rate since a filter can be replaced (to allow other filters to absorb $CO_2$ at its location), but it is not until it is regenerated that the CO2 can be captured, and filters that are replaced (e.g., daily replacement) accumulate before being transported for regeneration (see Supplementary Text 4 for more information). The results of the sensitivity analysis are shown in the tornado plot in Fig. S20.

The number of times the filter is regenerated per year has the largest impact on the $CO_2$ cost of capture. This highlights the importance of trying to replace and regenerate the filters at least once per week on average to keep $CO_2$ capture costs low. Filters that are not replaced weekly will take longer than 20 years to capture the maximum amount of $CO_2$ they can capture in their total useful lifetime. On the contrary, filters regenerated more than once per week on average means less filters sitting idle, which reduces $CO_2$ capture costs.

The second most sensitive variable is the filter cost. This is interesting because, while high filter costs make $CO_2$ capture less economic, lower filter manufacturing costs reflect potential cost reductions caused by a learning curve in manufacturing. The discount rate also has a significant impact on the $CO_2$ capture economics since filters are treated as CAPEX within the CO2 capture process, which involves a heavy expenditure in the first year; consequently, higher discount rates that place lower value in the later years impact the cost of capture significantly. This, however, highlights the potential of cheap capital (e.g., government-backed debt or green bonds) to significantly reduce the net cost of $CO_2$ capture, potentially helping it become economic. Finally, the electricity cost also has a significant impact on the capture economics, which highlights the importance of securing long-term PPAs, potentially from renewable electricity sources, at a price that favors the project economics.

It is worthwhile mentioning that, depending on the location this technology is implemented, some of the variables affecting the cost of $CO_2$ capture may vary significantly, among them electricity costs, the cost of filter manufacturing, and the availability of capital which affects the discount rate. While it may not be possible to model a scenario in every major region, the sensitivity of the net $CO_2$ capture costs to these major variables might help appreciate the effect of a particular location on net costs.

**Supplementary Text 6**

Uncertainty analysis

As a complement to the sensitivity analysis (Fig. S20), a Monte Carlo analysis was also conducted to estimate 95% confidence intervals for both the filter production costs and the net $CO_2$ cost of capture. Because the filter cost is also estimated here, the four raw materials that contribute the most to its cost were included in this analysis, namely the price of DME, ethanol, MEA, and N, N-dimethylformamide. A normal distribution was assumed for the price of each chemical, with the most recent market prices assumed as the mean cost for production. The standard deviation for the distribution was estimated as roughly one-fourth of the difference between the maximum and minimum price observed within the last 5 years, such that this range is covered in about 95% of cases.

Additional variables for the net cost of $CO_2$ captured considered are the electricity cost, average number of filter uses (and regeneration) per year, costs of $CO_2$ transportation, and costs of $CO_2$ storage. As with the previous variables, a normal distribution was assumed for the cost of electricity. For the other variables, where the underlying distribution is less known, a uniform distribution was assumed, where lower and upper bounds were selected based on an expected range of costs. A list of the variables and their assumed distributions are shown in Table S19. A total of 10,000 simulations were run as part of this analysis.

The results for the Monte Carlo simulation are shown in Fig. S21 and S22, for the filter production cost and the net cost of $CO_2$ capture, respectively. The average filter production cost obtained is \$18.1/kg, and we estimated a confidence interval of \$13.3-23.0/kg with 95% certainty. The average $CO_2$ capture net cost is \$185/tonne $CO_2$, and we estimated a confidence interval of \$120-260/tonne $CO_2$.

**Supplementary Text 7**

Additional commercialization considerations

As mentioned in the main manuscript, $CO_2$ capture costs through centralized DAC range between \$100/tonne and \$1000/tonne (*62*). This technology falls within that range in all cases, and even below the median, when solar regeneration is used.

When compared with technologies in the process of commercialization, such as those by Climeworks (*72*) and Carbon Engineering (*59*), this technology has an advantage in total energy consumption when the solar regeneration method is used, with a consumption 3.8 $GJ_e$/tonne $CO_2$; while most of the energy required for the other two processes is thermal, this could be a disadvantage if the goal is to minimize GHG emissions, requiring the use of synthetic natural gas or expensive electricity-to-heat technologies. Regarding process economics, Climeworks has reported capture costs between \$600/tonne $CO_2$ and \$1000/tonne $CO_2$ (*72*), which are above our estimates for this technology; however, a direct comparison cannot be made until a more detailed breakdown of the costs are released to the public. Carbon Engineering, on the other hand, has provided a breakdown by CAPEX, OPEX, and by type of energy used, with levelized costs ranging between \$113/tonne $CO_2$ and \$232/tonne $CO_2$ for a $CO_2$ product with a pressure high enough for transportation by pipeline (*59*). Their CAPEX per yearly $CO_2$ captured amount is between 2 and 3 times lower than the \$2,000 per yearly $CO_2$ captured we estimated in our work, mostly from the filter production. However, their analysis includes lower electricity costs of \$30-60/MWh; if an interpolation is made to consider the same discount rate (10%) and, similarly, the effect of electricity cost is linearly extrapolated to be the same as this work (\$83/MWh), Carbon Engineering's levelized cost of $CO_2$ capture is about \$150/tonne $CO_2$ and \$200 /tonne $CO_2$ for a process that uses heat and electricity or solely heat, respectively. This value is about half of our estimate of \$362/tonne $CO_2$ for $CO_2$ capture using solar regeneration, highlighting the importance of bringing filter manufacturing costs down, which currently account for 58% of the levelized cost.

Another factor that needs to be considered for commercialization purposes is potential revenue from emissions trading systems. In markets like Europe, the average price of credits since 2020 has been listed as \$68/tonne $CO_2$ in the primary market, and the price ranged between \$16/tonne $CO_2$ and \$111/tonne $CO_2$ between that time; in other markets, such as California, the average price since 2020 has been listed as \$28/tonne $CO_2$, and the price ranged between \$17/tonne $CO_2$ and \$42/tonne $CO_2$. While these prices are not enough to break even in net cost of $CO_2$ capture, it signals how much the net cost must be reduced before the technology is ready to market. Additional incentives through public policy might also facilitate commercialization. In the U.S., 45Q credits were updated recently to incentivize $CO_2$ capture both from point sources as well as DAC, and we have included them in this analysis. However, most DAC technologies are still uneconomic even with these incentives. For distributed air filter DAC, additional incentives might be required from city governments where the technology is adopted to convince people and businesses to participate. It is here where additional benefits such as lower $CO_2$ concentration within office space, or the potential to certify buildings as green or energy efficient could be used to promote adoption of this technology.

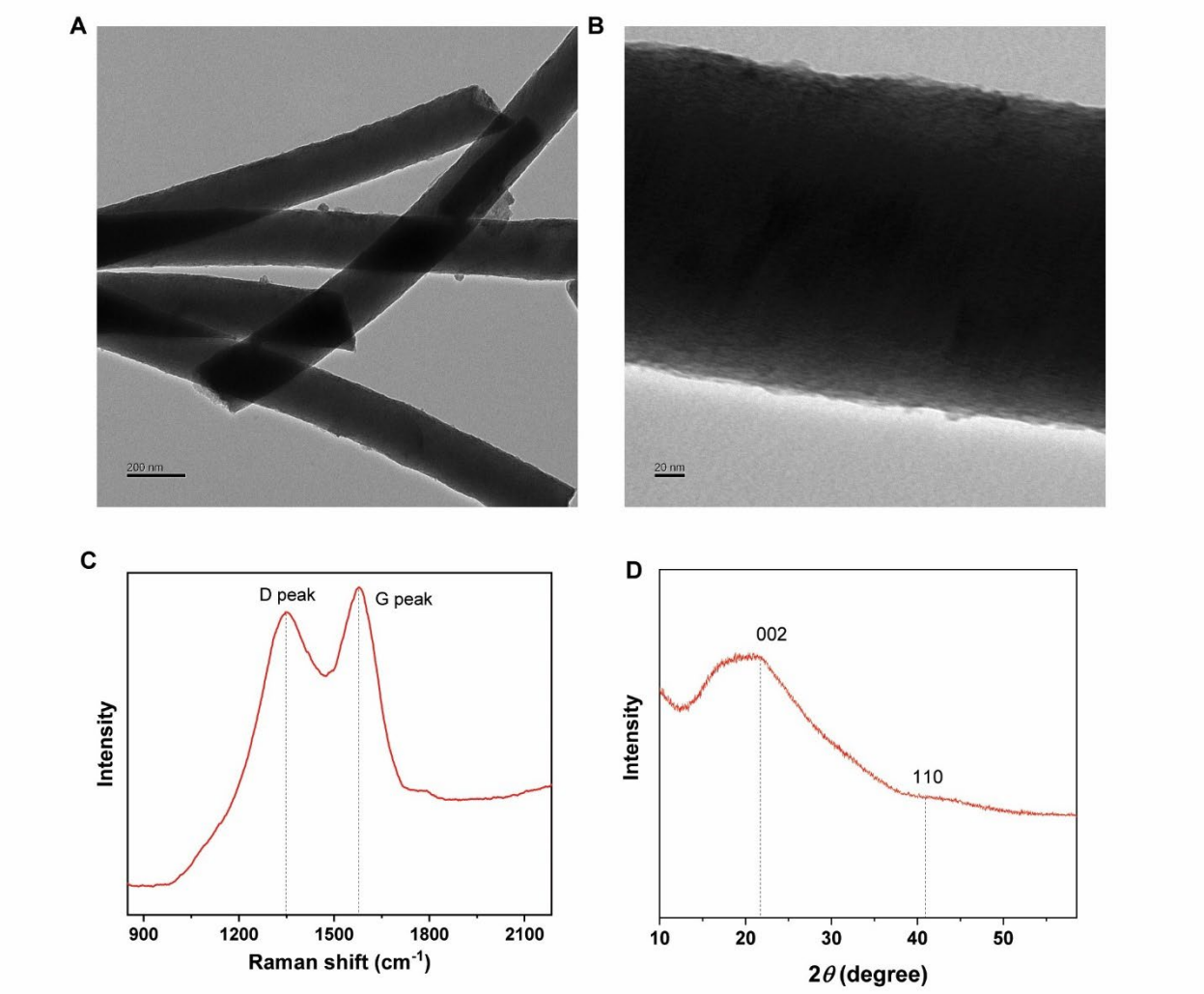


**Fig. S1. Characterization of CNF fibers.** (A-B) TEM image of the CNF fibers. (C) Raman and (D) XRD spectra of the CNF fibers.

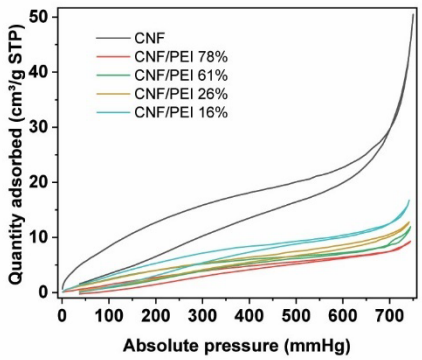


**Fig. S2. $N_2$ adsorption and desorption isotherms at -196˚C for CNFs and CNF/PEI adsorbents.**

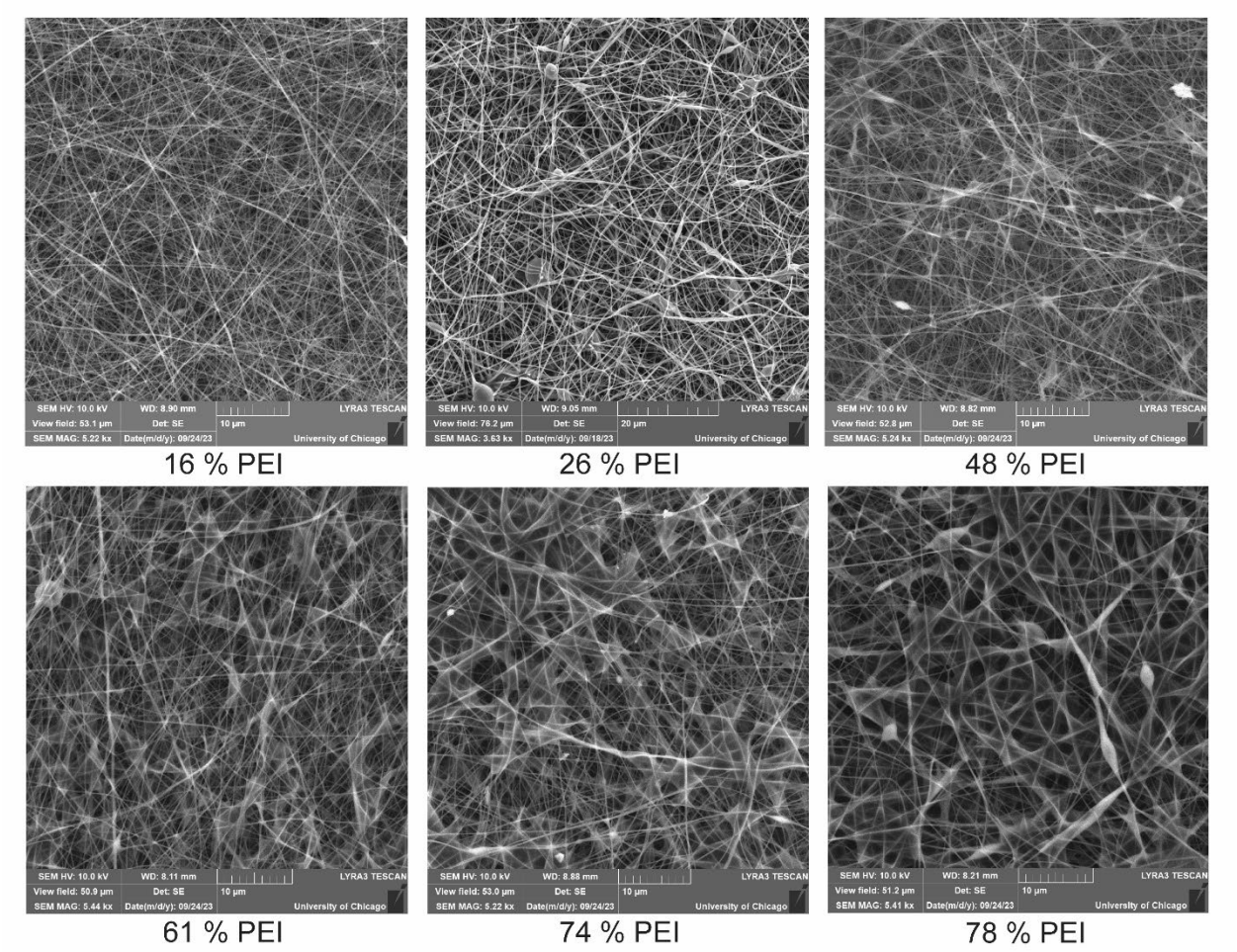


**Fig. S3. SEM images showing the morphology of CNF after impregnating PEI with different concentrations.**

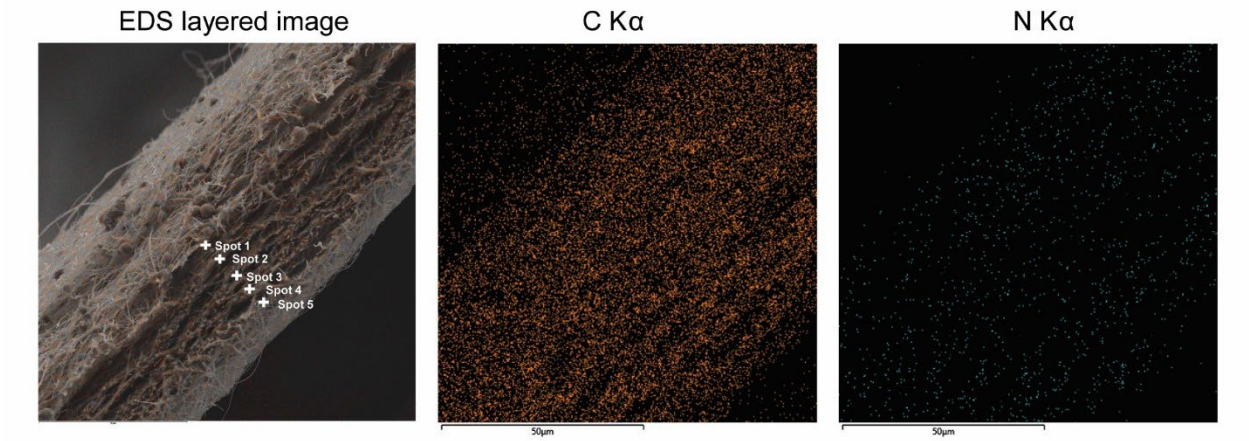


| | C | N | O |
|---|---|---|---|
| Spot 1 | 80.4 | 14.5 | 5.2 |
| Spot 2 | 87.7 | 8.9 | 3.5 |
| Spot 3 | 88.3 | 9.4 | 2.3 |
| Spot 4 | 83.5 | 12.9 | 3.6 |
| Spot 5 | 80.9 | 13.7 | 5.4 |

**Fig. S4. SEM image and EDS mapping of the side view of CNF/PEI adsorbent.** Quantitative measurements of C, N, and O elements at five different spots are summarized in the table.

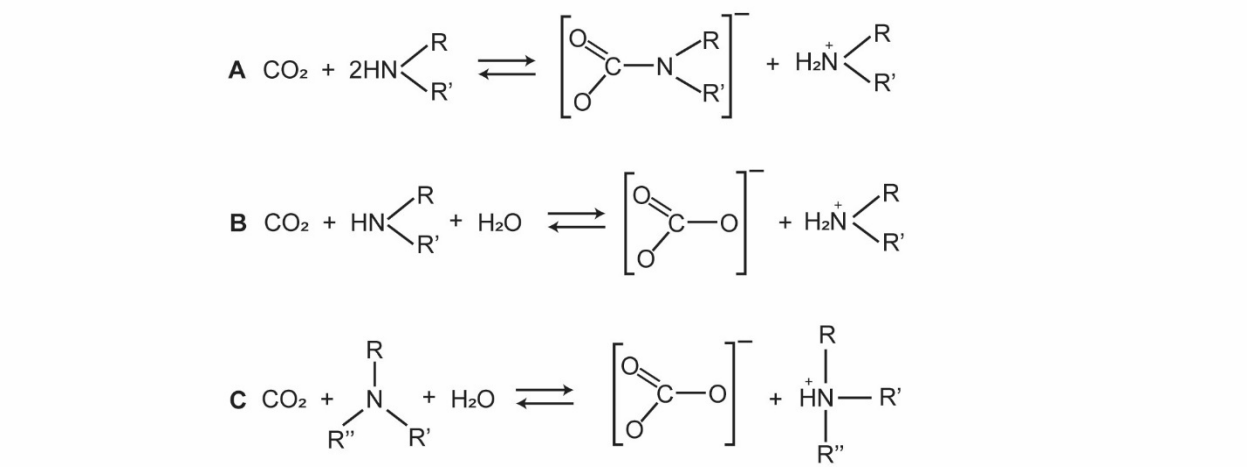


**Fig. S5. Mechanism of amine groups reacting with $CO_2$**. (A-B) Primary and secondary amine groups reacting with $CO_2$ (A) without the presence of $H_2O$, and (B) with the exitance of $H_2O$. (C) Tertiary amine groups reacting with $CO_2$ in the presence of $H_2O$.

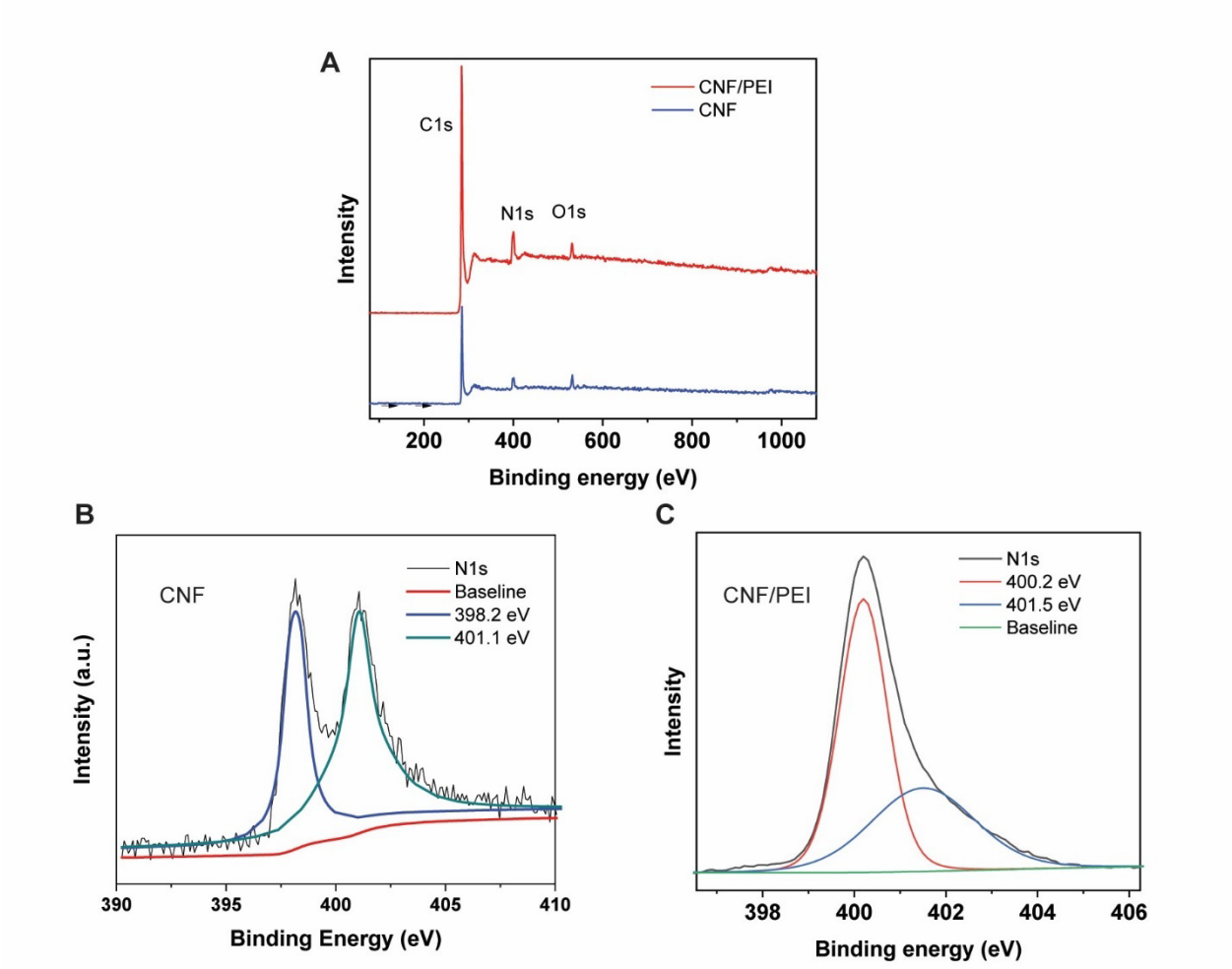


**Fig. S6. X-ray photoelectron spectra** of CNF and CNF/PEI. (A) Survey spectra and (B-C) high-resolution spectra of N1s.

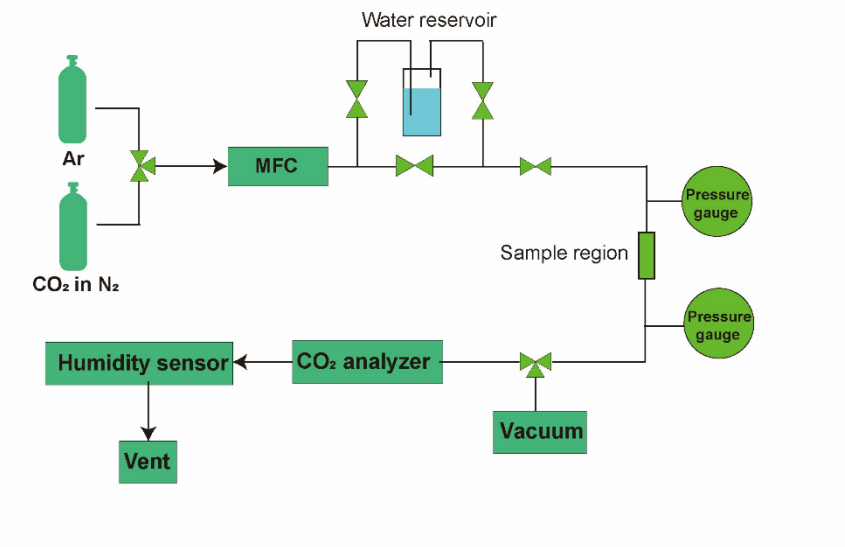


**Fig. S7. Setup for breakthrough tests and pressure drop measurements.**

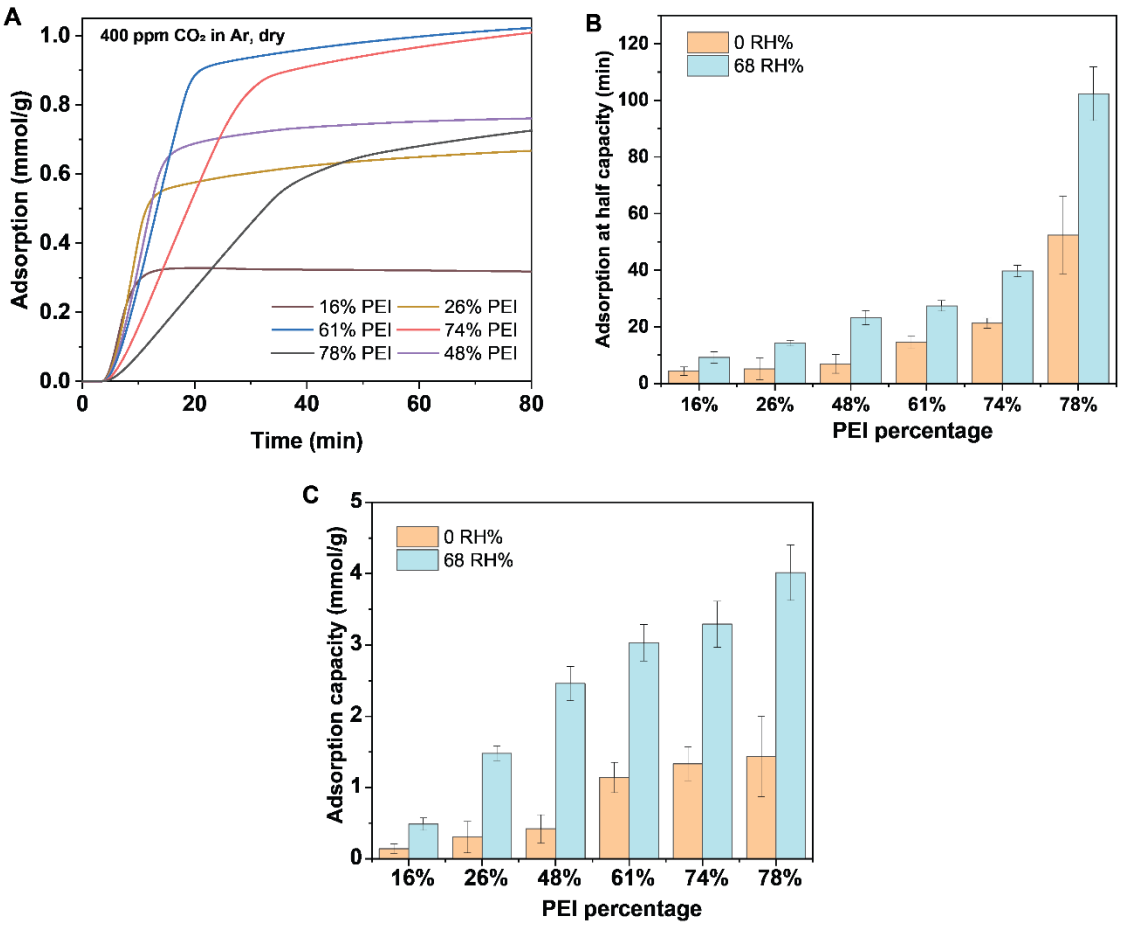


**Fig. S8. Adsorption capacity and kinetics of CNF-based adsorbent.** (A) Adsorption capacity in a dry environment derived from the breakthrough curves. (B) Adsorption time at half capacity for CNF adsorbents with different PEI mass loading. (C) Comparison of the adsorption capacity for CNF-based adsorbents at dry and wet environments.

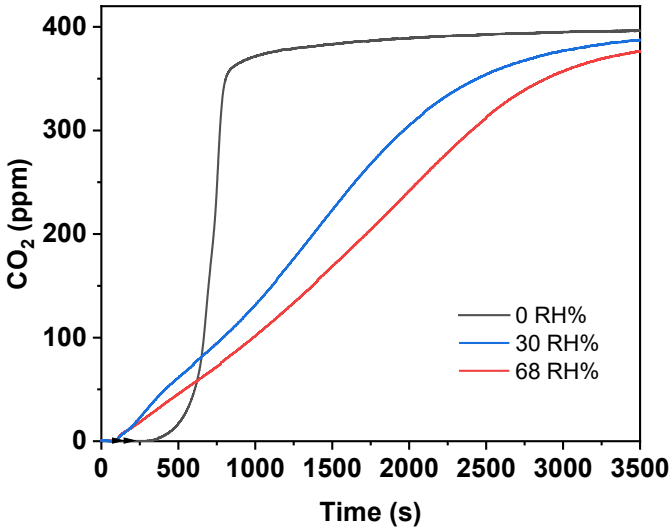


**Fig. S9. Breakthrough tests at three different humid conditions.**

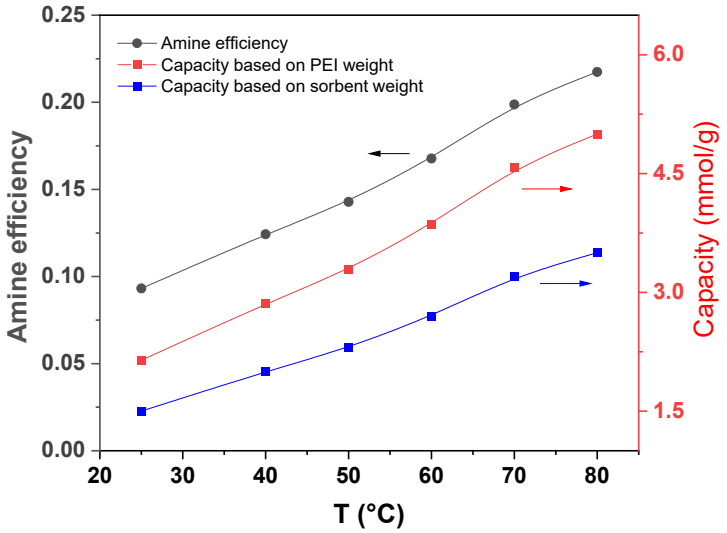


**Fig. S10. Adsorption capacity and amine efficiency at different temperatures.** The measurements are conducted using thermogravimetric analysis (TGA).

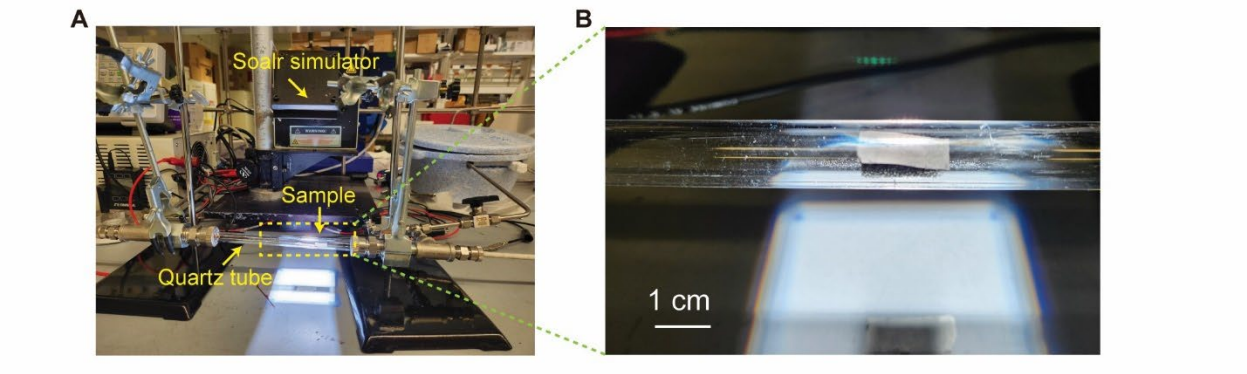


**Fig. S11. Setup for solar regeneration.** (A) Image of homebuilt setup equipped with a solar simulator for adsorbent regeneration. A quartz tube reactor containing the sample is irradiated by a solar simulator (AM 1.5G). The setup includes gas flow connections on both sides of the quartz tube. A $CO_2$ analyzer was connected downstream. (B) A close-up view of the sample placed inside the quartz tube under illumination.

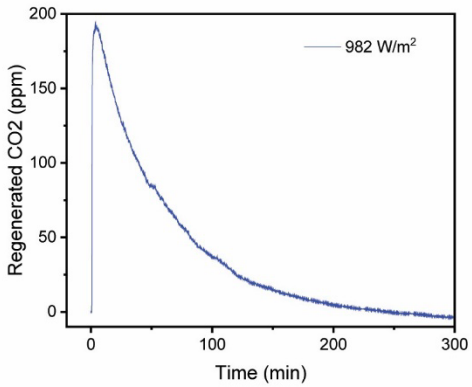


**Fig. S12. Regeneration of CNF-based DAC air filter under solar intensity of 982 W/m$^2$.**

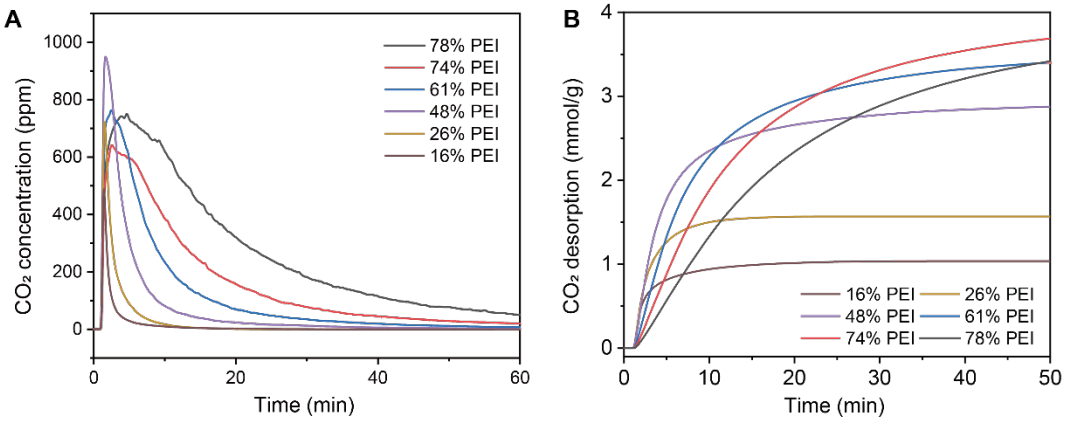


**Fig. S13. Adsorbent regeneration using solar thermal method.** (A) Detected $CO_2$ concentration by regenerating the CNF-based adsorbents with solar intensity of 1554 W/m$^2$. (B) Desorption capacity of CNF with different PEI mass loadings.

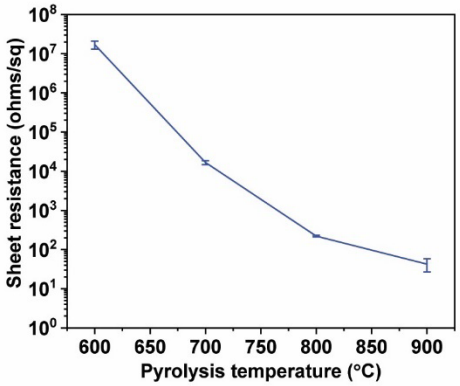


**Fig. S14. Sheet resistance of CNF prepared at different pyrolysis temperatures.**

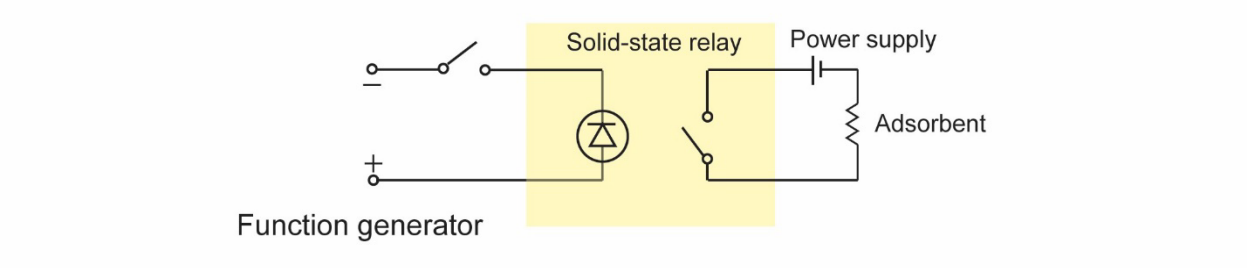


**Fig. S15. Electrical circuit for adsorbent regeneration by electrothermal method.**

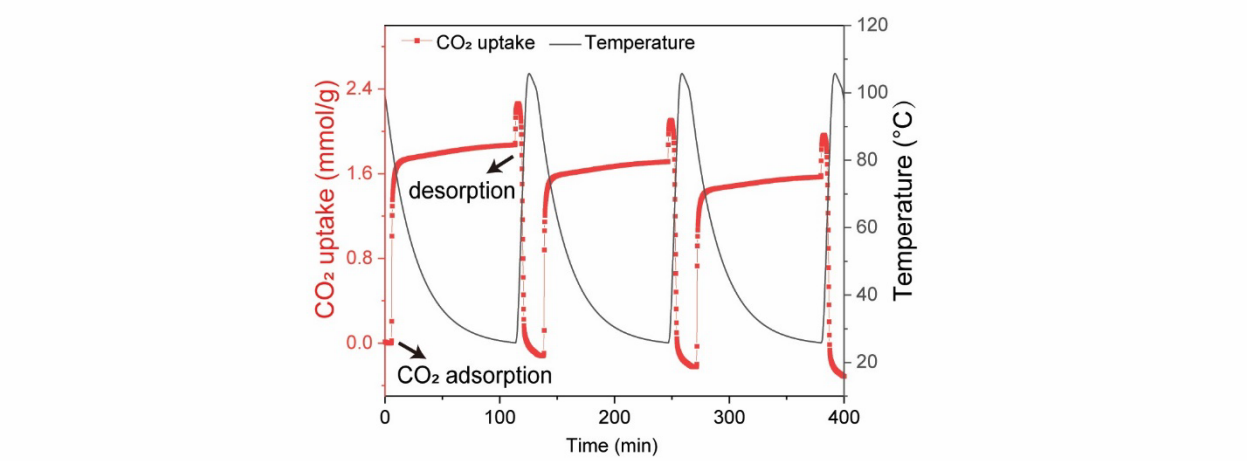


**Fig. S16. *In situ* measurement of $CO_2$ during the adsorption and desorption process using temperature swing by TGA.**

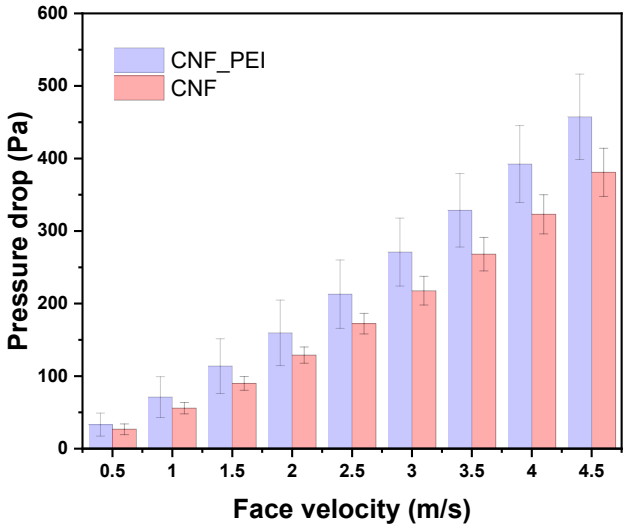


**Fig. S17. Pressure drop of air filters at different flow rates.**

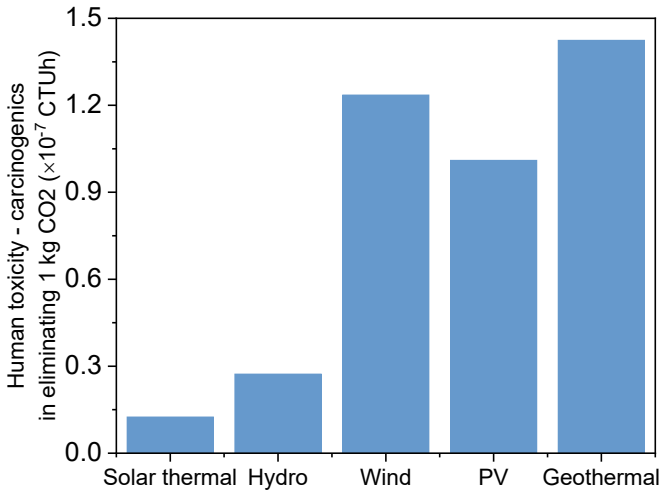


**Fig. S18. Human toxicity of the CNF-based adsorbent for eliminating 1kg $CO_2$ from direct air from cradle-to-grave.**

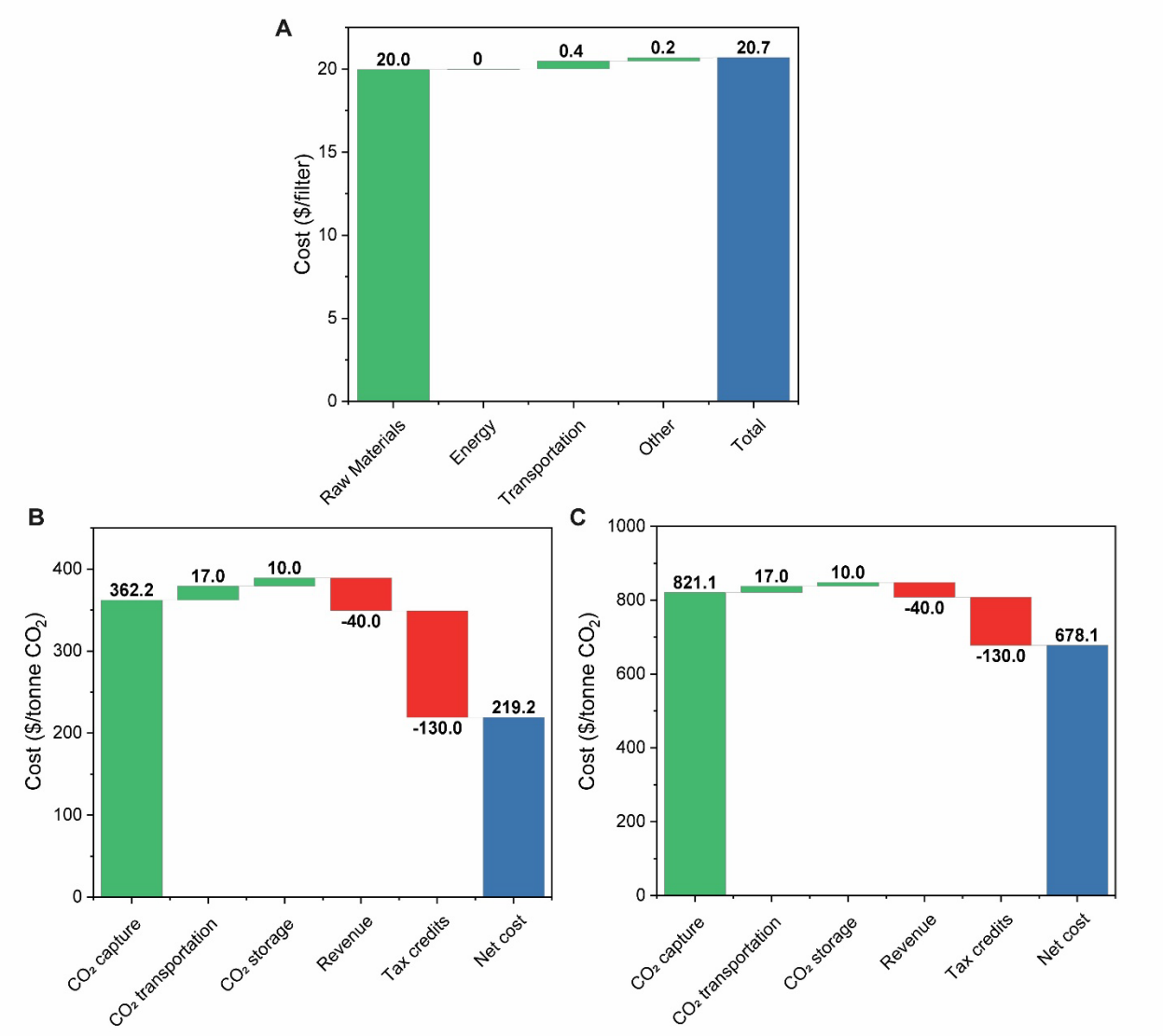


**Fig. S19. Cost estimation of the $CO_2$ capture and storage air filter.** (A) Levelized cost per filter broken down by its cost components. (B) Net cost of $CO_2$ used for EOR using solar regeneration. (C) Net cost of $CO_2$ used for EOR using electrothermal regeneration.

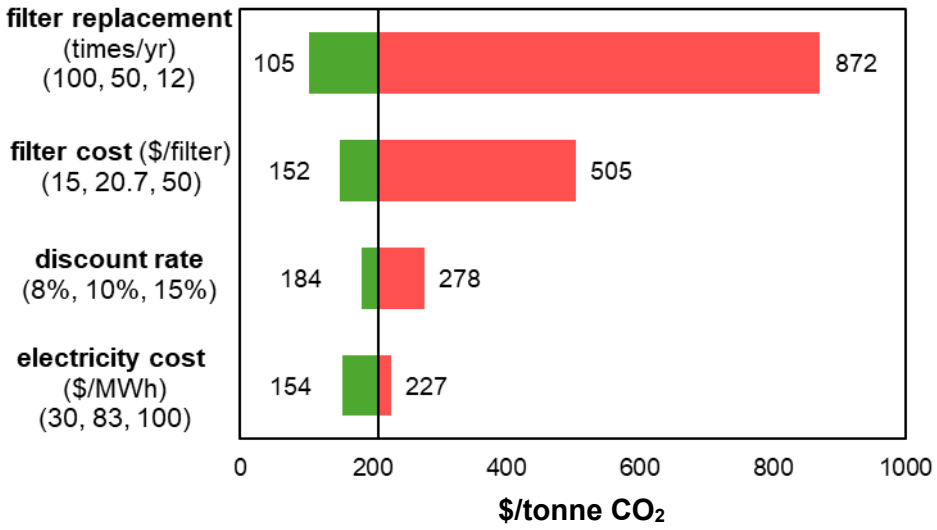


**Fig. S20. Sensitivity of net $CO_2$ cost of capture to key variables.**

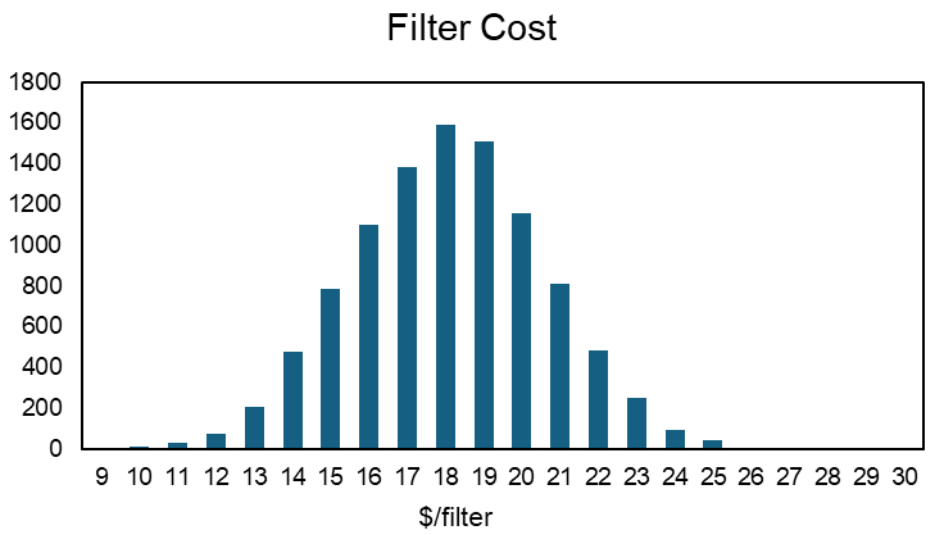


**Fig S21.** Filter production cost distribution for 10,000 simulations in Monte Carlo analysis.

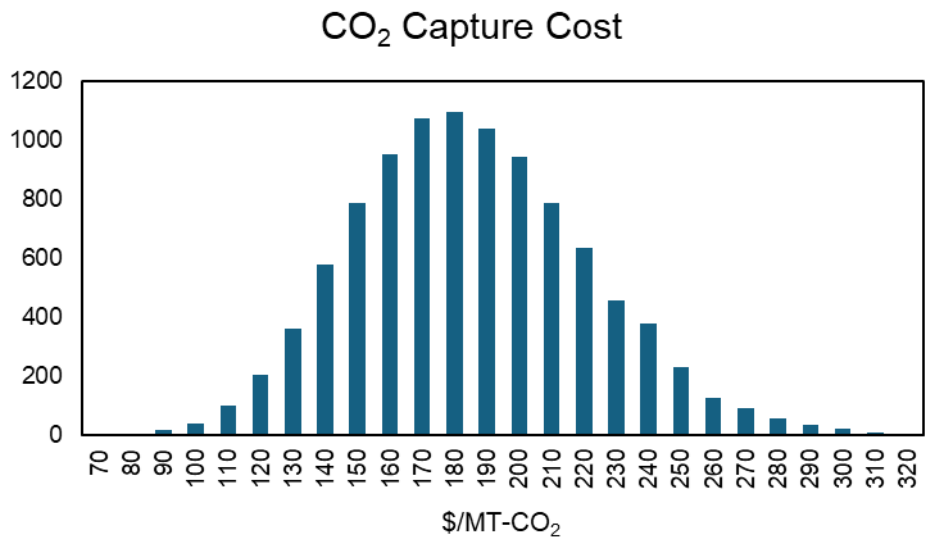


**Fig. S22**. Net $CO_2$ capture cost distribution for 10,000 simulations in Monte Carlo analysis.

**Table S1. Life cycle inventory (LCI) to produce 1 kg PEI.** PEI is fabricated by the homopolymerization of aziridine (*73*), produced via the Wenker process (*74*). The production is based on best-case reported by Deutz et al. (*54*)

| Flow | Dataset | Amount | Unit |
|---|---|---|---|
| **Input** | | | |
| Dimethyl ether[a] | Market for dimethyl ether \| dimethyl ether \| EN15804 | 13.58 | kg |
| Electricity, high voltage | Electricity, high voltage, production mix \| electricity, high voltage \| EN15804 | 0.42 | kWh |
| Ethanol, without water, in 99.7% solution state, from fermentation[a] | Dewatering of ethanol from biomass, from 95% to 99.7% solution state \| ethanol, without water, in 99.7% solution state, from fermentation \| EN15804 | 2.84 | kg |
| Heat, district or industrial, natural gas | Heat and power co-generation, natural gas, combined cycle power plant, 400 MW electrical \| heat, district, or industrial, natural gas \| EN15804 | 2.35 | MJ |
| Hydrochloric acid, without water, in 30% solution state | Market for hydrochloric acid, without water, in 30% solution state \| hydrochloric acid, without water, in 30% solution state \| EN15804 | 0.16 | kg |
| Monoethanolamine | Market for monoethanolamine \| monoethanolamine \| EN15804 | 1.42 | kg |
| Neutralising agent, sodium hydroxide-equivalent | Soda ash, light, crystalline, heptahydrate, to generic market for neutralising agent \| neutralising agent, sodium hydroxide-equivalent \| EN15804 | 2.02 | kg |
| Sulfuric acid | Market for sulfuric acid \| sulfuric acid \| EN15804 | 2.28 | kg |
| water, deionised | Water production, deionised \| water, deionised \| EN15804 | 11.99 | kg |
| **Output** | | | |
| **PEI** | | **1** | **kg** |
| Sodium sulfate, anhydrite | Market for sodium sulfate, anhydrite \| sodium sulfate, anhydrite \| EN15804 - RoW | 3.3 | kg |
| Spent solvent mixture | Market for spent solvent mixture \| spent solvent mixture \| EN15804 - RoW | 0.37 | kg |

**[a] Solvent recovery rate is 95%**

**Table S2. LCI for production of 1 kg PAN nanofiber.**

| Flow | Dataset | Amount | Unit |
|---|---|---|---|
| **Input** | | | |
| Ammonia, anhydrous, liquid | Market for ammonia, anhydrous, liquid \| ammonia, anhydrous, liquid \| EN15804 | 0.455 | kg |
| Electricity, high voltage | Electricity, high voltage, production mix \| electricity, high voltage \| EN15804 | 0.54 | MJ |
| Heat, district or industrial, natural gas | Heat and power co-generation, natural gas, conventional power plant, 100 MW electrical \| heat, district or industrial, natural gas \| EN15804 | 1.485 | MJ |
| Heat, district, or industrial, other than natural gas | Heat and power co-generation, oil \| heat, district or industrial, other than natural gas \| EN15804 | 0.83 | MJ |
| Heat, from steam, in the chemical industry | Market for heat, from steam, in chemical industry \| heat, from steam, in chemical industry \| EN15804 | 2 | MJ |
| Methyl methacrylate | Market for methyl methacrylate \| methyl methacrylate \| EN15804 | 0.05 | kg |
| N, N-dimethylformamide | Market for N,N-dimethylformamide \| N,N-dimethylformamide \| EN15804 | 11.5 | kg |
| Propylene | Market for propylene \| propylene \| EN15804 | 1.12 | kg |
| Sulfuric acid | Market for sulfuric acid \| sulfuric acid \| EN15804 | 0.01875 | kg |
| Water, deionised | Market for water, deionised \| water, deionised \| EN15804 | 2.125 | kg |
| **Output** | | | |
| Ammonia | | 0.00321 | kg |
| Ammonia, as N | | 0.01285 | kg |
| BOD5, Biological Oxygen Demand | | 0.03665 | kg |
| Chemical Oxygen Demand | | 0.03665 | kg |
| DOC, Dissolved Organic Carbon | | 0.011 | kg |
| **PAN nanofiber** | | **1** | **kg** |
| Propene | | 0.00003095 | kg |
| Propene | | 0.0124 | kg |
| Sulfate | | 0.03485 | kg |
| TOC, Total Organic Carbon | | 0.011 | kg |

**Table S3. LCI for production of 1 kg carbon nanofiber (CNF). The pyrolysis of CNF is based on Weber et al. (2018) (*75*).**

| Flow | Dataset | Amount | Unit |
|---|---|---|---|
| **Input** | | | |
| Heat, district or industrial, natural gas | Market for heat, district, or industrial, natural gas \| heat, district, or industrial, natural gas \| EN15804 | 2.81 | MJ |
| Heat, district or industrial, natural gas | Market group for heat, district, or industrial, natural gas \| heat, district, or industrial, natural gas \| EN15804 | 0.776 | MJ |
| Heavy fuel oil, burned in refinery furnace | Market for heavy fuel oil, burned in refinery furnace \| heavy fuel oil, burned in refinery furnace \| EN15804 | 0.0705 | MJ |
| PAN nanofiber | | 1.786 | kg |
| **Output** | | | |
| Carbon dioxide, fossil | | 1.17 | kg |
| **Carbon nanofiber** | | **1** | **kg** |
| Nitrogen | | 0.598 | kg |
| Water | | 0.589 | kg |

**Table S4. LCI for production of 1 kg silica based on Roes et al. (2010)(*76*).**

| Flow | Dataset | Amount | Unit |
|---|---|---|---|
| **Input** | | | |
| Heat, district or industrial, natural gas | Market for heat, district, or industrial, natural gas \| heat, district or industrial, natural gas \| EN15804 | 19.5 | MJ |
| Sodium silicate, solid | Market for sodium silicate, solid \| sodium silicate, solid \| EN15804 | 3.9 | kg |
| Sulfuric acid | Market for sulfuric acid \| sulfuric acid \| EN15804 | 0.66 | kg |
| Water, deionised | Market for water, deionised \| water, deionised \| EN15804 | 40 | kg |
| **Output** | | | |
| Particulates, < 2.5 um | | 0.0013 | kg |
| **Silica** | | **1** | **kg** |
| Sodium sulfate, anhydrite | | 0.96 | kg |
| Wastewater, average | | 0.035 | m3 |

**Table S5. LCI for production of 1 kg microcrystalline cellulose according to Husgafvel et al. (2016)(*77*).**

| Flow | Dataset | Amount | Unit |
|---|---|---|---|
| **Input** | | | |
| Ammonia, anhydrous, liquid | Ammonia production, partial oxidation, liquid \| ammonia, anhydrous, liquid \| EN15804 | 0.48 | kg |
| Electricity, high voltage | Electricity, high voltage, production mix \| electricity, high voltage \| EN15804 | 0.3 | kWh |
| Heat, district or industrial, natural gas | Market for heat, district, or industrial, natural gas \| heat, district or industrial, natural gas \| EN15804 | 29 | MJ |
| Hydrochloric acid, without water, in 30% solution state | Market for hydrochloric acid, without water, in 30% solution state \| hydrochloric acid, without water, in 30% solution state \| EN15804 | 1.48 | kg |
| Sulfate pulp, unbleached | Sulfate pulp production, from softwood, unbleached \| sulfate pulp, unbleached \| EN15804 | 1.11 | kg |
| Water, deionised | Market for water, deionised \| water, deionised \| EN15804 | 19.81 | kg |
| **Output** | | | |
| **Cellulose** | | **1** | **kg** |

**Table S6. LCI for end-of-life of the adsorbents.**

| Process | Dataset/Recycling rate |
|---|---|
| PEI on alumina | |
| PEI[a] | Market for spent anion exchange resin from potable water production \| spent anion exchange resin from potable water production \| EN15804 - RoW |
| Alumina[b] | 0.95 |
| PEI on Silica | |
| PEI[a] | Market for spent anion exchange resin from potable water production \| spent anion exchange resin from potable water production \| EN15804 - RoW |
| Silica[b] | 0.95 |
| PEI on CNF | |
| PEI[a] | Market for spent anion exchange resin from potable water production \| spent anion exchange resin from potable water production \| EN15804 - RoW |
| CNF[b] | 0.95 |
| PEI on cellulose | |
| PEI and cellulose | Market for spent anion exchange resin from potable water production \| spent anion exchange resin from potable water production \| EN15804 - RoW |

**[a] Treatment of PEI by incineration**

**[b] After burning the PEI, alumina, silica, and CNF can be recycled with a rate of 95%**

**Table S7. Energy type chosen for air filter system**

| Energy type | Dataset |
|---|---|
| Hydro | Electricity production, hydro, run-of-river \| electricity, high voltage \| EN15804 - US-NPCC |
| Wind | Electricity production, wind, <1MW turbine, onshore \| electricity, high voltage \| EN15804 - US-NPCC |
| Photovoltaic | Electricity production, photovoltaic, 3kwp slanted-roof installation, multi-Si, panel, mounted \| electricity, low voltage \| EN15804 - US-NPCC |
| Geothermal | Electricity production, deep geothermal \| electricity, high voltage \| EN15804 - US-HICC |

**Table S8. LCI for solar collector according to Mahmud et al. (*78*).**

| Flow | Dataset | Amount | Unit |
|---|---|---|---|
| **Input** | | | |
| Solar collector glass tube, with silver mirror | Market for solar collector glass tube, with silver mirror \| solar collector glass tube, with silver mirror \| EN15804 | 0.0003 | kg |
| **Output** | | | |
| **Solar collector** | | **1** | **Item(s)** |

**Table S9. LCI for air filter transportation in removing 1kg $CO_2$.**

| Flow | Dataset | Amount | Unit |
|---|---|---|---|
| **Input** | | | |
| Transport, freight, lorry, unspecified | Market for transport, freight, lorry, unspecified \| transport, freight, lorry, unspecified \| EN15804 | 0.1067 | t*km |
| Transport, pipeline, supercritical $CO_2$, 200km w recompression | Transport, pipeline, supercritical $CO_2$, 200 km w recompression | 0.2 | t*km |
| Transport, pipeline, supercritical $CO_2$, 200km w/o recompression | Transport, pipeline, supercritical $CO_2$, 200 km w/o recompression | 0.108 | t*km |
| **Output** | | | |
| **Transportation in removing 1 kg $CO_2$** | | **1** | **kg** |

**Table S10. LCI for transport, pipeline, supercritical $CO_2$, 200km w recompression**

| Flow | Dataset | Amount | Unit |
|---|---|---|---|
| **Input** | | | |
| Electricity, high voltage | Electricity, high voltage, production mix \| electricity, high voltage \| EN15804 | 0.03885 | kWh |
| Gas turbine, 10MW electrical | Gas turbine construction, 10 MW electrical \| gas turbine, 10 MW electrical \| EN15804 | 8.0416E-11 | Item(s) |
| Pipeline, supercritical $CO_2$/km | Pipeline, supercritical $CO_2$/km | 4.22797E-09 | km |
| **Output** | | | |
| **Transport, pipeline, supercritical $CO_2$, 200km w recompression** | | **1** | **t*km** |

**Table S11. LCI for transport, pipeline, supercritical $CO_2$, 200 km w/o recompression**

| Flow | Dataset | Amount | Unit |
|---|---|---|---|
| **Input** | | | |
| Pipeline, supercritical $CO_2$/km | Pipeline, supercritical $CO_2$/km | 4.22797E-09 | km |
| **Output** | | | |
| **Transport, pipeline, supercritical $CO_2$, 200 km w/o recompression** | | **1** | **t*km** |

**Table S12. LCI for drilling, deep borehole/m in $CO_2$ storage**

| Flow | Dataset | Amount | Unit |
|---|---|---|---|
| **Input** | | | |
| Activated bentonite | Activated bentonite production \| activated bentonite \| EN15804 | 20 | kg |
| Barite | Barite production \| barite \| EN15804 | 270 | kg |
| Cement, alternative constituents 21-35% | Cement production, alternative constituents 21-35% \| cement, alternative constituents 21-35% \| EN15804 | 200 | kg |
| Chemical, inorganic | Chemical production, inorganic \| chemical, inorganic \| EN15804 | 42.2 | kg |
| Chemical, organic | Chemical production, organic \| chemical, organic \| EN15804 | 9.05 | kg |
| Diesel, burned in diesel-electric generating set, 18.5kw | Diesel, burned in diesel-electric generating set, 18.5kw \| diesel, burned in diesel-electric generating set, 18.5kw \| EN15804 | 6300 | MJ |
| Lignite | Lignite mine operation \| lignite \| EN15804 | 0.2 | kg |
| Lubricating oil | Lubricating oil production \| lubricating oil \| EN15804 | 60 | kg |
| Steel, low-alloyed | Market for steel, low-alloyed \| steel, low-alloyed \| EN15804 | 210 | kg |
| Transport, freight train | Market for transport, freight train \| transport, freight train \| EN15804 | 487 | t*km |
| Transport, freight, lorry, unspecified | Market for transport, freight, lorry, unspecified \| transport, freight, lorry, unspecified \| EN15804 | 81.1 | t*km |
| **Output** | | | |
| Aluminium | | 0.06 | kg |
| AOX, Adsorbable Organic Halogen as Cl | | 0.000000478 | kg |
| Arsenic, ion | | 0.00042 | kg |
| Barium | | 0.006 | kg |
| BOD5, Biological Oxygen Demand | | 0.3 | kg |
| Boron | | 0.009 | kg |
| Calcium, ion | | 0.6 | kg |
| Chloride | | 6 | kg |
| Chromium, ion | | 0.0006 | kg |
| COD, Chemical Oxygen Demand | | 3 | kg |
| DOC, Dissolved Organic Carbon | | 0.3 | kg |
| drilling waste | Treatment of drilling waste, landfarming \| drilling waste \| EN15804 | 237 | kg |
| drilling waste | Treatment of drilling waste, residual material landfill \| drilling waste \| EN15804 | 158 | kg |

| | | | |
|---|---|---|---|
| **drilling, deep borehole/m** | | **1** | **m** |
| Fluoride | | 0.003 | kg |
| hazardous waste, for incineration | Market for hazardous waste, for incineration \| hazardous waste, for incineration \| EN15804 | 5 | kg |
| Hydrocarbons, aromatic | | 0.003 | kg |
| Iron, ion | | 0.18 | kg |
| Magnesium | | 0.12 | kg |
| Manganese | | 0.003 | kg |
| Methane, dichloro-, HCC-30 | | 0.06 | kg |
| Particulates, > 10 um | | 0.0148 | kg |
| Phosphorus | | 0.0012 | kg |
| Potassium, ion | | 0.9 | kg |
| Silicon | | 0.03 | kg |
| Sodium, ion | | 6 | kg |
| Strontium | | 0.018 | kg |
| Sulfur | | 0.12 | kg |
| TOC, Total Organic Carbon | | 0.3 | kg |
| Water, well, in ground | | 3.34 | $m^3$ |
| Zinc, ion | | 0.0012 | kg |

**Table S13. Sensitivity analysis of solvent use in adsorbent fabrication on the environmental impacts when capturing 1kg of $CO_2$.**

| Name | DMF | DMSO | Unit |
|---|---|---|---|
| Acidification | 2.78E-04 | 2.70E-04 | Mole H+ eq. |
| Climate change | 4.92E-02 | 4.43E-02 | kg $CO_2$ eq. |
| Freshwater ecotoxicity | 8.05E-01 | 7.58E-01 | CTUe |
| Freshwater eutrophication | 1.15E-05 | 1.01E-05 | kg P eq. |
| Human toxicity – carcinogenics | 2.76E-09 | 2.49E-09 | CTUh |
| Human toxicity – non-carcinogenics | 1.29E-08 | 1.20E-08 | CTUh |
| Ionizing radiation - ecosystems | 9.60E-09 | 7.54E-09 | CTUe |
| Ionizing radiation – human health | 2.98E-03 | 2.48E-03 | kg U235 eq. |
| Land use | 1.41E-02 | 1.32E-02 | kg SOC |
| Marine eutrophication | 1.34E-04 | 9.96E-05 | kg N eq. |
| Ozone depletion | 4.47E-09 | 3.82E-09 | kg CFC-11 eq. |
| Particulate matter/ Respiratory inorganics | 2.55E-05 | 2.33E-05 | kg PM2.5 eq. |
| Photochemical ozone formation | 1.39E-04 | 1.27E-04 | kg $C_2H_4$ eq. |
| Terrestrial eutrophication | 6.20E-04 | 5.63E-04 | Mole N eq. |

**Table S14. Sensitivity analysis of adsorbent cyclability on the environmental impacts for capturing 1kg of $CO_2$.**

| Name | 500 cycles | 1000 cycles | 2000 cycles | Unit |
|---|---|---|---|---|
| Acidification | 5.56E-04 | 2.78E-04 | 1.39E-04 | Mole H+ eq. |
| Climate change | 9.83E-02 | 4.92E-02 | 2.46E-02 | kg $CO_2$ eq. |
| Freshwater ecotoxicity | 1.61E+00 | 8.05E-01 | 4.03E-01 | CTUe |
| Freshwater eutrophication | 2.30E-05 | 1.15E-05 | 5.74E-06 | kg P eq. |
| Human toxicity - carcinogenics | 5.52E-09 | 2.76E-09 | 1.38E-09 | CTUh |
| Human toxicity – non-carcinogenics | 2.57E-08 | 1.29E-08 | 6.44E-09 | CTUh |
| Ionizing radiation - ecosystems | 1.92E-08 | 9.60E-09 | 4.80E-09 | CTUe |
| Ionizing radiation – human health | 5.97E-03 | 2.98E-03 | 1.49E-03 | kg U235 eq. |
| Land use | 2.83E-02 | 1.41E-02 | 7.07E-03 | kg SOC |
| Marine eutrophication | 2.68E-04 | 1.34E-04 | 6.69E-05 | kg N eq. |
| Ozone depletion | 8.94E-09 | 4.47E-09 | 2.24E-09 | kg CFC-11 eq. |
| Particulate matter/ Respiratory inorganics | 5.11E-05 | 2.55E-05 | 1.28E-05 | kg PM2.5 eq. |
| Photochemical ozone formation | 2.78E-04 | 1.39E-04 | 6.96E-05 | kg $C_2H_4$ eq. |
| Terrestrial eutrophication | 1.24E-03 | 6.20E-04 | 3.10E-04 | Mole N eq. |

**Table S15. Sensitivity analysis of adsorption capacity on the environmental impacts for capturing 1kg of $CO_2$.**

| Name | 2 mmol/g | 3 mmol/g | 4 mmol/g | Unit |
|---|---|---|---|---|
| Acidification | 3.41E-04 | 2.78E-04 | 2.39E-04 | Mole H+ eq. |
| Climate change | 6.25E-02 | 4.92E-02 | 4.07E-02 | kg $CO_2$ eq. |
| Freshwater ecotoxicity | 9.61E-01 | 8.05E-01 | 7.13E-01 | CTUe |
| Freshwater eutrophication | 1.43E-05 | 1.15E-05 | 9.72E-06 | kg P eq. |
| Human toxicity - carcinogenics | 3.46E-09 | 2.76E-09 | 2.32E-09 | CTUh |
| Human toxicity – non-carcinogenics | 1.54E-08 | 1.29E-08 | 1.14E-08 | CTUh |
| Ionizing radiation - ecosystems | 1.27E-08 | 9.60E-09 | 7.60E-09 | CTUe |
| Ionizing radiation – human health | 3.84E-03 | 2.98E-03 | 2.44E-03 | kg U235 eq. |
| Land use | 1.67E-02 | 1.41E-02 | 1.26E-02 | kg SOC |
| Marine eutrophication | 1.75E-04 | 1.34E-04 | 1.08E-04 | kg N eq. |
| Ozone depletion | 5.86E-09 | 4.47E-09 | 3.58E-09 | kg CFC-11 eq. |
| Particulate matter/ Respiratory inorganics | 3.19E-05 | 2.55E-05 | 2.16E-05 | kg PM2.5 eq. |
| Photochemical ozone formation | 1.74E-04 | 1.39E-04 | 1.17E-04 | kg $C_2H_4$ eq. |
| Terrestrial eutrophication | 7.63E-04 | 6.20E-04 | 5.32E-04 | Mole N eq. |

**Table S16. Financial assumptions in TEA model.**

| Financial Assumptions | |
|---|---|
| **Basis year** | 2024 |
| **Time horizon** | 20 years |
| **Nominal cost of equity** | 10% (*70*) |
| **Inflation** | 2.4% (*71*) |
| **Financing** | 100% equity |
| **Depreciation** | 20-year linear |
| **Tax rate** | 21% Federal<br>6% State |
| **Land CAPEX** | $100,000/acre<br>10 acres for filter production<br>10 acres for $CO_2$ regeneration |
| **Cost of electricity** | $82.6/MWh (*66*) |
| **Cost of heating** | $4/MMBtu (*67*) |
| **Filter transportation costs** | $0.28/ton-mi (*79*) |
| **$CO_2$ compression** | $24/tonne (*69*) |
| **$CO_2$ transportation** | $17/tonne (*68*) |
| **$CO_2$ storage** | $10/tonne (*68*) |
| **$CO_2$ sales** | $40/tonne (*80*) |
| **45Q credits (capture)** | $180/tonne (*56*) |
| **45Q credits (utilization)** | $130/tonne (*56*) |
| **Labor filter production** | 10 operators per shift<br>5 shifts per week<br>2080 hours per operator per year<br>$80/h for labor incl. overhead |
| **Labor $CO_2$ capture** | 4 operators per shift<br>5 shifts per week<br>2080 hours per operator per year<br>$80/h for labor incl. overhead |
| **Sales, general, and administrative (SG&A)** | 20% of labor |

**Table S17. Cost of raw materials.**

| Chemical | Cost ($/kg) |
|---|---|
| Dimethyl ether | 1.71 |
| Ethanol from fermentation | 0.46 |
| Hydrochloric acid 30% v/v | 0.23 |
| Monoethanolamine | 1.25 |
| Neutralizing agent, sodium hydroxide-equivalent | 0.31 |
| Sulfuric acid | 0.08 |
| Deionized water | 0.02 |
| Ammonia (anhydrous, liquid) | 0.50 |
| Methyl methacrylate | 1.97 |
| N, N-dimethylformamide | 8.00 |
| Propylene | 1.06 |

**Table S18. Cost of equipment.**

| Equipment | Cost ($/unit) | Number of Units | Source |
|---|---|---|---|
| 1200°C Controlled Atmosphere Muffle Furnace ETL/CE Certified | $7,990 | 62 | Market price |
| Thermo Scientific Lindberg/Blue M BF51766A Muffle Furnace | $4,040 | 62 | Market price |
| Electrospinning | $15,959 | 62 | Market price |
| Vacuum pump | $1,133,500 | 1 | Aspen Economic Analyzer |

**Table S19. Variable inputs to the Monte Carlo simulation and assumed distributions.**

| Variable | Distribution |
|---|---|
| DME cost | Normal distribution<br>Mean: \$1.4/kg<br>Standard deviation: \$0.3/kg |
| Ethanol Cost | Normal distribution<br>Mean: \$0.46/kg<br>Standard deviation: \$0.12/kg |
| MEA cost | Normal distribution<br>Mean: \$1.25/kg<br>Standard deviation: \$0.5/kg |
| N, N-dimethylformamide cost | Normal distribution<br>Mean: \$8/kg<br>Standard deviation: \$0.5/kg |
| Electricity cost | Normal distribution<br>Mean: \$82/MWh<br>Standard deviation: \$10/MWh |
| Filter average uses per year | Uniform distribution<br>Minimum: 40<br>Maximum: 60 |
| $CO_2$ transportation | Uniform distribution<br>Minimum: \$10/tonne $CO_2$<br>Maximum: \$30/tonne $CO_2$ |
| $CO_2$ storage | Uniform distribution<br>Minimum: \$8/tonne $CO_2$<br>Maximum: \$20/tonne $CO_2$ |

## REFERENCES AND NOTES


1. H. Wang, J. Liu, M. Klaar, A. Chen, L. Gudmundsson, J. Holden, Anthropogenic climate change has influenced global river flow seasonality. *Science* **383**, 1009–1014 (2024).

2. A. Momeni, R. V. McQuillan, M. S. Alivand, A. Zavabeti, G. W. Stevens, K. A. Mumford, Direct air capture of $CO_2$ using green amino acid salts. *Chem. Eng. J.* **480**, 147934 (2024).

3. Z. Liu, Z. Deng, S. Davis, P. Ciais, Monitoring global carbon emissions in 2022. *Nat. Rev. Earth Environ.* **4**, 205–206 (2023).

4. K. S. Lackner, S. Brennan, J. M. Matter, A.-H. A. Park, A. Wright, B. Van Der Zwaan, The urgency of the development of $CO_2$ capture from ambient air. *Proc. Natl. Acad. Sci. U.S.A.* **109**, 13156–13162 (2012).

5. E. S. Sanz-Pérez, C. R. Murdock, S. A. Didas, C. W. Jones, Direct capture of $CO_2$ from ambient air. *Chem. Rev.* **116**, 11840–11876 (2016).

6. J. K. Soeherman, A. J. Jones, P. J. Dauenhauer, Overcoming the entropy penalty of direct air capture for efficient gigatonne removal of carbon dioxide. *ACS Eng. Au* **3**, 114–127 (2023).

7. E. National Academies of Sciences, and Medicine, *Negative Emissions Technologies and Reliable Sequestration: A Research Agenda* (National Academies Press, 2019).

8. M. Ozkan, S. P. Nayak, A. D. Ruiz, W. Jiang, Current status and pillars of direct air capture technologies. *iScience* **25**, 103990 (2022).

9. T. A. Jacobson, J. S. Kler, M. T. Hernke, R. K. Braun, K. C. Meyer, W. E. Funk, Direct human health risks of increased atmospheric carbon dioxide. *Nat. Sustain.* **2**, 691–701 (2019).

10. M. Benammar, A. Abdaoui, S. H. Ahmad, F. Touati, A. Kadri, A modular IoT platform for real-time indoor air quality monitoring. *Sensors* **18**, 581 (2018).

11. M. Kang, Y. Yan, C. Guo, Y. Liu, X. Fan, P. Wargocki, L. Lan, Ventilation causing an average $CO_2$ concentration of 1,000 ppm negatively affects sleep: A field-lab study on healthy young people. *Build. Environ.* **249**, 111118 (2024).

12. C. Sui, J. Pu, T.-H. Chen, J. Liang, Y.-T. Lai, Y. Rao, R. Wu, Y. Han, K. Wang, X. Li, V. Viswanathan, P.-C. Hsu, Dynamic electrochromism for all-season radiative thermoregulation. *Nat. Sustain.* **6**, 428–437 (2023).

13. Y. Dong, M. Coleman, S. A. Miller, Greenhouse gas emissions from air conditioning and refrigeration service expansion in developing countries. *Annu. Rev. Env. Resour.* **46**, 59–83 (2021).

14. N. El Hadri, D. V. Quang, E. L. V. Goetheer, M. R. M. Abu Zahra, Aqueous amine solution characterization for post-combustion $CO_2$ capture process. *Appl. Energy* **185**, 1433–1449 (2017).

15. S. Zhou, X. Chen, T. Nguyen, A. K. Voice, G. T. Rochelle, Aqueous ethylenediamine for $CO_2$ capture. *ChemSusChem* **3**, 913–918 (2010).

16. H. Seo, T. A. Hatton, Electrochemical direct air capture of $CO_2$ using neutral red as reversible redox-active material. *Nat. Commun.* **14**, 313 (2023).

17. A. Hemmatifar, J. S. Kang, N. Ozbek, K. J. Tan, T. A. Hatton, Electrochemically mediated direct $CO_2$ capture by a stackable bipolar cell. *ChemSusChem* **15**, e202102533 (2022).

18. J. H. Rheinhardt, P. Singh, P. Tarakeshwar, D. A. Buttry, Electrochemical capture and release of carbon dioxide. *ACS Energy Lett.* **2**, 454–461 (2017).

19. R. Sharifian, R. Wagterveld, I. Digdaya, C. Xiang, D. Vermaas, Electrochemical carbon dioxide capture to close the carbon cycle. *Energ. Environ. Sci.* **14**, 781–814 (2021).

20. P. Zhu, Z.-Y. Wu, A. Elgazzar, C. Dong, T.-U. Wi, F.-Y. Chen, Y. Xia, Y. Feng, M. Shakouri, J. Y. Kim, Continuous carbon capture in an electrochemical solid-electrolyte reactor. *Nature* **618**, 959–966 (2023).

21. J. C. Abanades, Y. A. Criado, H. I. White, Direct capture of carbon dioxide from the atmosphere using bricks of calcium hydroxide. *Cell Rep. Phys. Sci.* **4**, 101339 (2023).

22. Z. Li, X. Guo, X. Xue, X. Xu, B. Wang, Investigations on kinetics and mechanisms of $CaCO_3$ calcination in calcium looping. *Ind. Eng. Chem. Res.* **62**, 4851–4863 (2023).

23. J. Blamey, E. Anthony, J. Wang, P. Fennell, The calcium looping cycle for large-scale $CO_2$ capture. *Prog. Energy Combust. Sci.* **36**, 260–279 (2010).

24. H. Mao, J. Tang, G. S. Day, Y. Peng, H. Wang, X. Xiao, Y. Yang, Y. Jiang, S. Chen, D. M. Halat, A scalable solid-state nanoporous network with atomic-level interaction design for carbon dioxide capture. *Sci. Adv.* **8**, eabo6849 (2022).

25. G. Zainab, A. A. Babar, N. Iqbal, X. Wang, J. Yu, B. Ding, Amine-impregnated porous nanofiber membranes for $CO_2$ capture. *Compos. Commun.* **10**, 45–51 (2018).

26. G. N. Short, E. Burentugs, L. Proaño, H. J. Moon, G. Rim, I. Nezam, A. Korde, S. Nair, C. W. Jones, Single-walled zeolitic nanotubes: advantaged supports for poly(ethylenimine) in $CO_2$ separation from simulated air and flue gas. *JACS Au* **3**, 62–69 (2023).

27. Y. Labreche, R. P. Lively, F. Rezaei, G. Chen, C. W. Jones, W. J. Koros, Post-spinning infusion of poly(ethyleneimine) into polymer/silica hollow fiber sorbents for carbon dioxide capture. *Chem. Eng. J.* **221**, 166–175 (2013).

28. A. Goeppert, M. Czaun, R. B. May, G. S. Prakash, G. A. Olah, S. Narayanan, Carbon dioxide capture from the air using a polyamine based regenerable solid adsorbent. *J. Am. Chem. Soc.* **133**, 20164–20167 (2011).

29. H. A. Evans, D. Mullangi, Z. Deng, Y. Wang, S. B. Peh, F. Wei, J. Wang, C. M. Brown, D. Zhao, P. Canepa, Aluminum formate, $Al(HCOO)_3$: An earth-abundant, scalable, and highly selective material for $CO_2$ capture. *Sci. Adv.* **8**, eade1473 (2022).

30. S. He, B. Zhu, X. Jiang, G. Han, S. Li, C. H. Lau, Y. Wu, Y. Zhang, L. Shao, Symbiosis-inspired de novo synthesis of ultrahigh MOF growth mixed matrix membranes for sustainable carbon capture. *Proc. Natl. Acad. Sci. U.S.A.* **119**, e2114964119 (2022).

31. M. Fasihi, O. Efimova, C. Breyer, Techno-economic assessment of $CO_2$ direct air capture plants. *J. Clean. Prod.* **224**, 957–980 (2019).

32. D. V. Quang, A. V. Rabindran, N. El Hadri, M. R. Abu-Zahra, Reduction in the regeneration energy of $CO_2$ capture process by impregnating amine solvent onto precipitated silica. *Eur. Sci. J.* **9**, 82–102 (2013).

33. D. T. Nguyen, R. Truong, R. Lee, S. A. Goetz, A. P. Esser-Kahn, Photothermal release of $CO_2$ from capture solutions using nanoparticles. *Energ. Environ. Sci.* **7**, 2603–2607 (2014).

34. P. Li, T.-J. Zhao, J.-H. Zhou, Z.-J. Sui, Y.-C. Dai, W.-K. Yuan, Characterization of carbon nanofiber composites synthesized by shaping process. *Carbon* **43**, 2701–2710 (2005).

35. X. Shen, H. Du, R. H. Mullins, R. R. Kommalapati, Polyethylenimine applications in carbon dioxide capture and separation: From theoretical study to experimental work. *Energ. Technol.* **5**, 822–833 (2017).

36. R. B. Said, J. M. Kolle, K. Essalah, B. Tangour, A. Sayari, A unified approach to $CO_2$–amine reaction mechanisms. *ACS Omega* **5**, 26125–26133 (2020).

37. J. Yu, S. S. Chuang, The structure of adsorbed species on immobilized amines in $CO_2$ capture: An in situ IR study. *Energy Fuel* **30**, 7579–7587 (2016).

38. U. Tumuluri, M. Isenberg, C.-S. Tan, S. S. Chuang, In situ infrared study of the effect of amine density on the nature of adsorbed $CO_2$ on amine-functionalized solid sorbents. *Langmuir* **30**, 7405–7413 (2014).

39. W. Zhang, H. Liu, Y. Sun, J. Cakstins, C. Sun, C. E. Snape, Parametric study on the regeneration heat requirement of an amine-based solid adsorbent process for post-combustion carbon capture. *Appl. Energy* **168**, 394–405 (2016).

40. N. Iqbal, X. Wang, J. Yu, B. Ding, Robust and flexible carbon nanofibers doped with amine functionalized carbon nanotubes for efficient $CO_2$ capture. *Adv. Sustain. Syst.* **1**, 1600028 (2017).

41. M. Al-Marri, M. Khader, M. Tawfik, G. Qi, E. Giannelis, $CO_2$ sorption kinetics of scaled-up polyethylenimine-functionalized mesoporous silica sorbent. *Langmuir* **31**, 3569–3576 (2015).

42. W. Sagues, H. Jameel, D. Sanchez, S. Park, Prospects for bioenergy with carbon capture & storage (BECCS) in the United States pulp and paper industry. *Energ. Environ. Sci.* **13**, 2243–2261 (2020).

43. F. Rezaei, R. P. Lively, Y. Labreche, G. Chen, Y. Fan, W. J. Koros, C. W. Jones, Aminosilane-grafted polymer/silica hollow fiber adsorbents for $CO_2$ capture from flue gas. *ACS Appl. Mater. Interfaces* **5**, 3921–3931 (2013).

44. D. V. Quang, A. Dindi, M. R. Abu-Zahra, One-step process using $CO_2$ for the preparation of amino-functionalized mesoporous silica for $CO_2$ capture application. *ACS Sustain. Chem. Eng.* **5**, 3170–3178 (2017).

45. H. V. Thakkar, A. J. Ruba, J. A. Matteson, M. P. Dugas, R. P. Singh, Accelerated testing of PEI-silica sorbent pellets for direct air capture. *ACS Omega* **9**, 45970–45982 (2024).

46. G. Qi, Y. Wang, L. Estevez, X. Duan, N. Anako, A.-H. A. Park, W. Li, C. W. Jones, E. P. Giannelis, High efficiency nanocomposite sorbents for $CO_2$ capture based on amine-functionalized mesoporous capsules. *Energ. Environ. Sci.* **4**, 444–452 (2011).

47. Y. Bian, L. Zhang, C. Chen, Experimental and modeling study of pressure drop across electrospun nanofiber air filters. *Build. Environ.* **142**, 244–251 (2018).

48. X. Zhao, S. Wang, X. Yin, J. Yu, B. Ding, Slip-effect functional air filter for efficient purification of PM2. 5. *Sci. Rep.* **6**, 35472 (2016).

49. R. Schäppi, D. Rutz, F. Dähler, A. Muroyama, P. Haueter, J. Lilliestam, A. Patt, P. Furler, A. Steinfeld, Drop-in fuels from sunlight and air. *Nature* **601**, 63–68 (2022).

50. M. L. Godec, V. A. Kuuskraa, P. Dipietro, Opportunities for using anthropogenic $CO_2$ for enhanced oil recovery and CO2 storage. *Energy Fuel* **27**, 4183–4189 (2013).

51. Q. Zhu, Developments on $CO_2$-utilization technologies. *Clean Energy* **3**, 85–100 (2019).

52. Y. Zhang, C. Jackson, S. Krevor, An estimate of the amount of geological $CO_2$ storage over the period of 1996–2020. *Environ. Sci. Technol. Lett.* **9**, 693–698 (2022).

53. S. Krevor, H. de Coninck, S. E. Gasda, N. S. Ghaleigh, V. de Gooyert, H. Hajibeygi, R. Juanes, J. Neufeld, J. J. Roberts, F. Swennenhuis, Subsurface carbon dioxide and hydrogen storage for a sustainable energy future. *Nat. Rev. Earth Environ.* **4**, 102–118 (2023).

54. S. Deutz, A. Bardow, Life-cycle assessment of an industrial direct air capture process based on temperature–Vacuum swing adsorption. *Nat. Energy* **6**, 203–213 (2021).

55. T. Terlouw, K. Treyer, C. Bauer, M. Mazzotti, Life cycle assessment of direct air carbon capture and storage with low-carbon energy sources. *Environ. Sci. Technol.* **55**, 11397–11411 (2021).

56. J. A. Yarmuth, H.R.5376 - 117th Congress (2021-2022): Inflation Reduction Act of 2022 (2022); www.congress.gov/bill/117th-congress/house-bill/5376.

57. Standard 62. 2–2013 Ventilation for Acceptable Indoor Air Quality (ANSI/ASHRAE, 2013); https://ierga.com/wp-content/uploads/sites/2/2017/10/ASHRAE-62.2-2013.pdf.

58. N. Muscatiello, A. McCarthy, C. Kielb, W. H. Hsu, S. A. Hwang, S. Lin, Classroom conditions and $CO_2$ concentrations and teacher health symptom reporting in 10 New York State Schools. *Indoor Air* **25**, 157–167 (2015).

59. D. W. Keith, G. Holmes, D. S. Angelo, K. Heidel, A process for capturing $CO_2$ from the atmosphere. *Joule* **2**, 1573–1594 (2018).

60. H. Li, M. E. Zick, T. Trisukhon, M. Signorile, X. Liu, H. Eastmond, S. Sharma, T. L. Spreng, J. Taylor, J. W. Gittins, Capturing carbon dioxide from air with charged-sorbents. *Nature* **630**, 654–659 (2024).

61. L. Sabantina, M. Klöcker, M. Wortmann, J. R. Mirasol, T. Cordero, E. Moritzer, K. Finsterbusch, A. Ehrmann, Stabilization of polyacrylonitrile nanofiber mats obtained by needleless electrospinning using dimethyl sulfoxide as solvent. *J. Ind. Text* **50**, 224–239 (2020).

62. R. Chauvy, L. Dubois, Life cycle and techno-economic assessments of direct air capture processes: An integrated review. *Int. J. Energy Res.* **46**, 10320–10344 (2022).

63. G. Zang, P. Sun, E. Yoo, A. Elgowainy, A. Bafana, U. Lee, M. Wang, S. Supekar, Synthetic methanol/Fischer–Tropsch fuel production capacity, cost, and carbon intensity utilizing $CO_2$ from industrial and power plants in the United States. *Environ. Sci. Technol.* **55**, 7595–7604 (2021).

64. A. Sinha, L. A. Darunte, C. W. Jones, M. J. Realff, Y. Kawajiri, Systems design and economic analysis of direct air capture of $CO_2$ through temperature vacuum swing adsorption using MIL-101(Cr)-PEI-800 and mmen-Mg2(dobpdc) MOF adsorbents. *Ind. Eng. Chem. Res.* **56**, 750–764 (2017).

65. "National assessment of geologic carbon dioxide storage resources: summary," (2013); https://pubs.usgs.gov/publication/fs20133020.

66. U.S. Energy Information Administration, "Form EIA-861M, Monthly Electric Power Industry Report" (2025); www.eia.gov/electricity/monthly/epm_table_grapher.php?t=epmt_5_6_a.

67. U.S. Energy Information Administration, "Short-Term Energy Outlook" (2025); www.eia.gov/outlooks/steo/.

68. E. Smith, J. Morris, H. Kheshgi, G. Teletzke, H. Herzog, S. Paltsev, The cost of $CO_2$ transport and storage in global integrated assessment modeling. *Int. J. Greenh. Gas Control* **109**, 103367 (2021).

69. S. Hughes, A. Zoelle, M. Woods, S. Henry, S. Homsy, S. Pidaparti, N. Kuehn, H. Hoffman, K. Forrest, A. Sheriff, T. Fout, W. Summers, S. Herron, "Cost of capturing CO2 from industrial sources" (DOE/NETL-2022/3319, National Energy Technology Laboratory, 2022); https://doi.org/10.2172/1887586.

70. A. Damodaran, Cost of equity and capital (US) (Damodaran Online, 2025); https://pages.stern.nyu.edu/~adamodar/New_Home_Page/datafile/wacc.html.

71. Federal reserve bank of St. Louis, 10-year breakeven inflation rate (2025); https://fred.stlouisfed.org/series/T10YIE.

72. A. Pujol, M. Heuckendorff, T. Helmer Pedersen, Techno-economic analysis of two novel direct air capture-to-urea concepts based on process intensification. *J. Clean. Prod.* **496**, 144932 (2025).

73. A. von Harpe, H. Petersen, Y. Li, T. Kissel, Characterization of commercially available and synthesized polyethylenimines for gene delivery. *J. Control. Release* **69**, 309–322 (2000).

74. G. W. Meijer, G. Kanny, J. F. Briois, *Ullmann's encyclopedia of industrial chemistry* (Wiley, 2000).

75. S. Weber, J. F. Peters, M. Baumann, M. Weil, Life cycle assessment of a vanadium redox flow battery. *Environ. Sci. Technol.* **52**, 10864–10873 (2018).

76. A. Roes, L. Tabak, L. Shen, E. Nieuwlaar, M. Patel, Influence of using nanoobjects as filler on functionality-based energy use of nanocomposites. *J. Nanopart. Res.* **12**, 2011–2028 (2010).

77. R. Husgafvel, K. Vanhatalo, L. Rodriguez-Chiang, L. Linkosalmi, O. Dahl, Comparative global warming potential assessment of eight microcrystalline cellulose manufacturing systems. *J. Clean. Prod.* **126**, 620–629 (2016).

78. M. P. Mahmud, N. Huda, S. H. Farjana, C. Lang, Environmental impacts of solar-photovoltaic and solar-thermal systems with life-cycle assessment. *Energies* **11**, 2346 (2018).

79. Volpe National Transportation Systems Center, "National Transportation Statistics 2021 [50th Anniversary Edition]" (Bureau of Transportation Statistics, 2021); https://doi.org/10.21949/1523389.

80. V. Núñez-López, E. Moskal, Potential of $CO_2$-EOR for near-term decarbonization. *Front. Clim.* **1**, 5 (2019).